Electrically Conductive Adhesives (ECAs)

James E. Morris (jmorris@cecs.pdx.edu)
Department of Electrical & Computer Engineering, Portland State University, Oregon, USA
Johan Liu (johan.liu@pe.chalmers.se)
Department of Production Engineering, Chalmers University of Technology, Goteborg, Sweden

Contents

I. Introduction
- A. Technology Drivers
- B. Isotropic Conductive Adhesives (ICAs)
- C. Anisotropic Conductive Adhesives (ACAs)
- D. Non-Conductive Adhesive (NCA.)

II. Structure
- A. ICA
- B. ACA
- C. Modelling

III. Materials and Processing
- A. Polymers
- B. ICA Filler
- C. ACA Processing

IV. Electrical Properties
- A. ICA
  1. Percolation theory
  2. Inter-particle conduction
  3. Intra-particle resistance
  4. Contact resistance
- B. Electrical Measurements
- C. ACA

V. Mechanical Properties
- A. ICA
- B. ACA

VI. Thermal Properties
- A. Thermal Characteristics
- B. Maximum Current Carrying Capacity

VII. Reliability
- A. ICA
  1. Cure schedule
  2. Moisture effects
  3. Galvanic corrosion
  4. Thermo-mechanical
- B. ACA
- C. General Comments

VIII. Environmental Impact
IX. Further Study
X. References

I. Introduction

A. Technology Drivers

There are two primary categories of Electrically Conductive Adhesive (ECA):

- Isotropic Conductive Adhesive (ICA)
- Anisotropic Conductive Adhesive (ACA).
- ACAs are available as paste (ACP) or film (ACF).

Both types conduct through metal filler particles in an adhesive polymer matrix.

ECAs have been used for electronics packaging applications for decades in hybrid, die-attach and display assembly. ICAs have been used extensively for die attach, and in automotive electronics. ACF technology is employed with almost every liquid crystal display. But there has been growing interest from the electronics industry over the past decade or so in other kinds of electronics packaging applications. While toxicity issues and environmental incompatibility of the lead in tin-lead solders triggered that greater interest at the outset, it has been the other evident advantages which continue to drive further research. ECAs can offer the following additional potential advantages:

- Fine-pitch capability, especially when using ACAs for flip-chip
- Elimination of underfilling with ACA bonding;
- Low temperature processing capability;
- Flexible, simple processing and hence low cost.

In addition, solder failures due to the formation of voids or brittle intermetallics are controlled by diffusion rates at small dimensions, and time-to-failure scales as the square of the dimensions, limiting solder reliability lifetimes at ultra-fine pitch [1].

ACF has long been the interconnect of choice in the LCD display industry, and ACP is now finding applications in flex circuits and surface mount technology (SMT) for chip-scale package (CSP), ASIC, and flip chip attachment for cell phones, radios, PDAs, laptop PCs, and cameras. ICAs are used extensively in die-attach, for many years for small passive chip attachment in automotive electronics, and in varied consumer products, e.g. in Matsushita/Panasonic's stud bump joints. More recent applications include RFID tags, potentially for the antenna as well as chip connections.

This chapter presents an overview of the current status of understanding of conductive adhesives in various electronics packaging applications, and of some fundamental issues relevant to their continuing development. It is organized with initial discussions of basic ECA concepts of structure-related properties, and how these are affected by material selection and processing, followed by general properties and reliability considerations. In each section, there is material common to both ICAs and ACAs, and parallel treatments of topics specific to each.

B. Isotropic Conductive Adhesives (ICAs)

Ag is usually used as the filler material due to its high conductivity and simple processing for ICA applications. Figure 1 shows the microstructure of an ICA joint, (a) in schematic form, (b) for a flip chip component, and (c) for SMT attachment, (both on FR-4 substrates.) The metallic filler content is high enough (between 25-30 volume percent) to cause direct metallic contact from bump or lead to circuit board pad.

C. Anisotropic Conductive Adhesives (ACAs)

Polymer based metal-plated spheres or Ni fillers are mainly used for ACA applications. In an ACA joint, the filler particles normally constitute between 5-10 volume percent, and do not cause any direct metallic contact. It is only after the application of pressure during curing that electrical conduction becomes possible in the normal (z-axis) direction, as is illustrated in Figure 2. The Ni particles are usually matched to soft Au contacts, and the contact deforms to define the contact area. By contrast, the polymer beads, usually Au-plated, deform to establish bump and pad contacts. As there is no direct contact between the particles, ACA technology is very suitable for fine pitch assembly, and is starting to find applications in flip-chip technology.

D. Non-Conductive Adhesive (NCA.)

The complementary NCA technology is mentioned only briefly here, for completeness. In this case, the contacts themselves are in direct metal-to-metal contact, held together by the NCA. The concept relies upon surface asperities for the direct contacts.

II. Structure

A. ICA

As the proportion of metal in the ICA polymer matrix is increased, (Figure 3,) the resistance drops only slightly until the "percolation threshold" is reached, when the first continuous metal path is established through the composite material [2]. The resistance continues to drop more slowly as multiple parallel paths are developed with the continued addition of more metal filler. Ideally one would like to use the minimum quantity of filler necessary to pass the threshold, but in practice manufacturing tolerances require a design target composition significantly beyond the threshold. Very small contact volumes increase the statistical spread of resistivities already inherent in a percolation structure. Minimal filler content is a requirement for both economic reasons (since Ag is expensive) and to maximize the proportion of polymer adhesive. Both issues can be addressed by the use of metal flakes (or rods) as filler instead of spheres. The benefits can be readily understood by considering the extreme case of flakes of zero thickness, which would clearly establish a percolation threshold at zero metal content, i.e. at 100% adhesive with zero filler cost. Practical commercial materials achieve substantial reduction in the threshold composition by the use of flakes, by virtue of the increased connectivity which accompanies the increased surface-to-volume ratio, compounded by bi-modal particle size distributions (Figure 4.) The efficacy of bi-modal particle distributions has been demonstrated [3] and either flakes or powders can be used for the smaller particles [4].

Theoretical simulation has been carried out to optimize the electrical performance of a conductive adhesive joint using a bimodal distribution of metal fillers using computer modeling with finite-element analysis. Two classes of metal fillers were used, i.e. nano-scale and micro-scaled particles. The goal was to decrease the metal loading to improve the mechanical performance for specified electrical properties. It has been shown that it is possible to decrease the total metal loading with good electrical conductivity using a bimodal filler distribution [5], but that the nano-particles increase resistivity for a given total filler content, due to mean free path limits and increased numbers of contacts.

In addition, the flakes at the material surfaces seem to be aligned parallel to the surface to a depth of a few flake thicknesses (Figure 4.) The effect seems to be universal, with squeegee or syringe dispensation, and also appears inside air bubbles, probably due to surface tension [6]. One also sees particle alignment inside the material, parallel to the contacts, if pressure is applied [7], as seen in Figure 1(b). Particulate orientations are important for predictions of both adhesive strength and electrical resistance. Flow modeling of the ICA under stencil, print, or dispensation, and/or positioning pressure is much more difficult than underfill flow modeling [8] due to filler sizes and shapes. Recently, a dynamic model of the effects of compression has demonstrated flake alignment quite dramatically [9].

There are various novel approaches to the improvement of electrical connectivity at a given metal content, including magnetic alignment of nickel filler rods [10], the use of polymer particles to force z-axis alignment of flakes [11], and electric fields [12]. Anything that increases the packing density/efficiency of the particles also increases the connectivity and reproducibility of the structure, permitting the design composition to move closer to the percolation threshold, and a reduction in metal filler.

Modelling of the material structure for prediction of the electrical properties has included

- Distributions of uniformly sized spheres [13]
- 2D [14] and 3D [15] rectangular particles with limited size distributions and x, y, z orientations
- Rectangular particles rotated about the x, y, z axes in 1° increments [16].

The extension to bimodal flake representations requires a dramatic increase in computing power. The difficulty lies in the development of an efficient algorithm for the random placement of the particles, which must not impinge upon the space occupied by another. As the structure fills up, this process becomes more and more time consuming. A potential energy technique has proved effective [16], but the most recent advances have been by the use of compression algorithms applied to initially well separated particles [9, 17, 18].

B. ACA

The first structural issue for ACAs is the distribution of particles, and how many are captured and compressed between the contacts. A software package has been developed to calculate the average resistance of the ACA contacts for pastes or randomly loaded ACFs [19], with statistical distribution. Input parameters include particle size and distribution, particle loading, pad size and pad spacings. The program also performs the inverse calculations, i.e it determines the particle loading requirements for a specified minimum number of particles per pad, (i.e. minimum conductance.)

It is implicit in the program above that the particle distribution is well behaved, but for pastes, the realities of flow around and over pads as pressure is applied will dramatically alter the distribution. So the program has only been validated against ACFs, and studies on the entrapment of particles between pads continue. There have been efforts made to model ACP flow [20], and the problem should be more tractable than underfill flow modeling [8], due to the smaller particles, but there appears to be no result yet suitable for inclusion into a particle distribution model.

There is, of course, a finite probability that there are no particles in the joint. Williams et al tried to estimate this by assuming the particles are placed in the bonding area according to the Poisson distribution [21]:

$$P(n) = \frac{e^{-\mu}\mu^{n}}{n!} \qquad (1)$$

where P is the probability of an open joint, n is the number of particles per pad, and μ is the average number particles on a pad, given by:

$$\mu = \frac{3Af}{2\pi r^{2}} \qquad (2)$$

where A is the total bonding area, f is the volume fraction of the particles, and r is the radius of the particle. So, for a typical volume fraction ranging from 3 to 15 vol. %, chip area (100 mm^2) and pad size (100 μm^2), the probability for an ACA open circuit is

$$P(0) = e^{-\mu} = e^{-\frac{3Af}{2\pi r^{2}}} \qquad (4)$$

which gives 10^{-13} to 10^{-3} for typical parameters, i.e. extremely small. However, in reality, there is always a crowding effect which must be taken into account. In this case, the particle distribution can be described using a binominal distribution model [21]:

$$P(n) = C_n^N (1-s)^{N-n} s^n \qquad (5)$$

where N is the maximum number of particles that can be contained in an area A, C_n^N is the binominal coefficient, and s is equal to f/f_m where f_m is the volume fraction corresponding to maximum packing. In the limit when $f<<1$, equations (4) and (5) give identical results for P(0).

Bridging is possible due to there being too many particles between contacts, or insufficient contact separation, as illustrated in Figure 5 [23, 24]. The probability for bridging is given as

$$p = 1 - \left(1 - \left(\frac{6f}{\pi}\right)^{\frac{d}{4r^2}}\right)^{\frac{hl}{4r^2}} \qquad (6)$$

where f is the volume fraction of the particles, h is the pad height, l the pad length, d the spacing between the pads, and r is the radius of the particle. Bridging probabilities are also very small, as seen for various cases in Figure 6, where it is clearly shown that the lowest combined probability for bridging and skipping occurs in the volume fraction between 7 and 15% depending on what model we use. This volume fraction range is also generally used for commercial ACA materials today.

C. Modeling

The goal of any physical modeling exercise is to demonstrate that the physical processes are well understood. Validation is achieved by agreement of the model predictions with experimental data. It is clear for both ICAs and ACAs, that successful comparisons of electrical modeling with experimental results require accurate structural modeling first. For ICAs, there have been some superficial efforts at structural modeling in the past, and as a result, comparisons of electrical models with experiment were either strictly qualitative [14, 15] or subject to parameter adjustment to achieve a fit [16]. For ACAs, one

would expect less difficulty in structural characterization, and the general form of the match of theory to experiment for the resistance variation with pressure [25] is convincing, even recognizing the need for fitting parameters. For ICAs, similar results are achievable for "dry" test systems [10], i.e. without epoxy, but cannot be correlated with actual ICA internal pressures because these are unknown. Real progress in realistic ICA structural modeling has bee made only recently [9, 18].

III. Materials and Processing

A. Polymers

The polymers in common use in ECAs are thermoset epoxies, with sufficient thermoplastic mixed in to allow for softening and release for rework under moderate heat. Up until now, the polymers used in ICAs have been adapted from those developed for other purposes. Recent research has provided clear pointers to the properties required of the new generation of materials, but the engineering trade-offs make implementation difficult, and the universal solution has yet to appear on the market. Certainly, the need for mechanical energy dissipative materials is well known, and the search for new materials must focus on this property, but without compromising on others. Polymer adhesion is a fundamental property which must be understood, with fundamental contact angle wetting experiments for ICA base polymers a first step.

The cure process has been modeled successfully by very simple mathematical expressions [26, 27], which do however require accurately determined parameters from experimental Differential Scanning Calorimetry (DSC) data. For reaction rate

$$d\alpha/dt = k\, f(\alpha), \qquad (7)$$

where α = degree of cure, $k = A \exp(-E/kT)$ is the chemical rate constant, and $f(\alpha)$ is a function of the reactant concentration, given by

$$f(\alpha) = (1 - \alpha)^n \qquad (8)$$

for an n-th order model, the degree of cure is calculated as:

1st order $d\alpha/dt = k(1- \alpha)$ $\alpha = 1-\exp(-kt)$ (9)

2nd order $d\alpha/dt = k(1- \alpha)^2$ $\alpha = 1 - (1 + kt)^{-1}$ (10)

etc. More complex treatments employ a linear combination with the auto-catalyzed model

$$d\alpha/dt = k\, f(\alpha) = (k_1 + k_2\, \alpha^m)(1- \alpha)^n \qquad (11)$$

The success is demonstrated by the observation of the sudden decrease in ICA resistance (Figure 7) at the predicted point of 100% cure [6, 27] according to equation 9. The assumption is that the resistance drop is due to physical shrinkage of the polymer matrix approaching complete cure, but this particular property, i.e. physical shrinkage and the development of an internal pressure to squeeze filler particles together, has not been measured, and does not appear to have been modeled. The measurement of a dimensional shrinkage with cure should not be a major problem, nor should the measurement of internal pressures.

Prior to the initiation of cure, however, the carrier solvents which permit the ICA paste (or ACP) to be printed must be expelled. Failure to do so degrades reliability, adhesion, and impact strength. The problem arises when partially cured polymer traps the evaporating solvent in bubbles. Brief exposure to vacuum prior to cure visibly decreases ICA paste volume as gas escapes from the surface [28], but the more practical technique is a pre-cure heat soak, e.g. for about 20-30 minutes at 100-120°C [29] which achieves the same result and marked reliability improvement.

ICAs typically cure at around 150°C for 20-30 minutes. This is considered too long to be competitive with solders [30], but there are much faster "snap-cure" alternatives.

B. ICA Filler

The metal filler of choice has been Ag, but the warning that Ag is accompanied by electromigration problems keeps on coming up. Certainly the existence of the electromigration problem has been documented [31], but it does not seem to be a problem in practice. It is evident in un-cured material [12], and it has been suggested that commercial additives to the polymer seal the silver surface, defeating migration tendencies. There also appears to be a field threshold, and moisture is requisite, but systematic study is required to establish the boundaries to the effect. In addition, the diffusion and clustering of metals in polymers is well established [32, 33], and should be investigated for Ag in appropriate polymers as the limiting zero-field phenomenon. Sencaktar et al have recently correlated electromigration with Ag surface pitting [34].

There have also been materials reported using low melting point alloys [35, 36], or Sn-coated Ag particles [37]. The intent is for the particles to form metallurgical bonds during the polymer cure, to achieve lower contact resistances. The greater rigidity of the metallic network could be a problem if the contacts fracture under mechanical stress, but apparently the Sn inhibits Ag migration [37].

C. ACA Processing

ACA assembly typically requires a thermode for the bonding process, which takes place in about 30 seconds. Many parameters can affect the bonding quality during the ACA bonding process:

- Curing temperature and time of the ACA
- Bonding temperature and time
- Temperature ramp rate
- Alignment accuracy
- Pressure value, pressure distribution & pressure application rate
- Bump height and uniformity
- Board planarity and stiffness

If the thermal ramp rate is too high, no particle contact will occur as the adhesive will be cured during the bonding process, before the pad and bump can both reach the particles.

The effect of bump to pad alignment accuracy is mainly related to the performance of the bonder. A normal flip-chip bonder that offers a 5μm alignment accuracy is usually good enough. The question is how much tolerance is acceptable for the ACA bonding. As has been discussed earlier, the particle location will affect the electrical conduction performance of the joint, and bad alignment will have the same effect.

ACA flow during bonding has also been modelled by Mannan et al [38]. A typical situation of the particle flow is shown in Figure 8. Assuming Newtonian flow

$$\tau_{xy} = \eta \, \delta\gamma/\delta t \qquad (12)$$

where τ_{xy} is the shear stress, $\delta\gamma/\delta t$ is the strain rate, and η is the viscosity. By solving the Navier-Stokes equation in this condition, one can obtain the following equation that describes the pressure under the chip during the bonding due to the flow of the ACA:

$$P = 2F/(\pi R^2)(1 - r^2/R^2) \qquad (13)$$

where F is the bonding force, r is the distance from the chip center, and R is half of the edge length of the chip. Pressure variations cause planarity problems during the bonding. In reality, the ACA resin probably follows a power law type of flow as

$$\tau_{xy} = \eta_0 (d\gamma/dt)^n \qquad (14)$$

where n is the power law index and η_0 is the viscosity of the fluid. In this case, Mannan et al have successfully obtained the following equation to predict the time for the ACA to be squeezed out between the chip and substrate:

$$Tp = (2n+1)/(n+1)[2\pi \eta_0^{(n+3)}/(F(n+3)h_0^{(n+1)})]^{1/n}[(h_0/h)^{(n+1)/n} - 1] \qquad (15)$$

where h is the ACA height. One of the important issues here is that the viscosity of the ACA will increase dramatically when it starts to get cured. This can be described as

$$\eta_0 = \eta_{00} e^{-b(T-T_0)} \qquad (16)$$

Where b and η_{00} are constants and T_0 is an arbitrary reference temperature. However, measuring the viscosity of the ACA material close to the curing point remains a problem.

IV. Electrical Properties

A. ICA

The electrical resistance of the ICA has four distinct components [2]. Three of these are obvious; they are the metal "intra-particle" resistance, the "inter-particle" contact resistance, and the "contact" resistance between the surface particles and the lead or contact pad. The fourth component comes from the

meandering "percolation" path of the continuous metallic connection(s) through the material. Figure 9 illustrates the principle, showing how some metal particles carry current, while others do not.

(1) *Percolation theory* is well developed for the elementary system of uniform conducting spheres (or cubes) in a perfectly insulating medium [39]. There are no analytical solutions, and the theoretical results are deduced by the averaging of multiple Monte Carlo randomized simulations. Conducting particles are randomly assigned to sites on a specified regular array. For any realistic random system, the site separations must be much less than the particle sizes, and the problem becomes how to fit new particles into the structure at high particle concentrations (as required here) with reasonable efficiency.

The percolation modeling literature commonly includes finite intra-particle resistivities, but inter-particle resistances are seen less often. This is partly because the most common systems of interest would assume electron tunneling between particles, and the exponential dependence of the tunneling probability on separation introduces a strong parametric dependence on a poorly characterized variable. Percolation models of the electrical resistance of ICA systems have included both intra-particle and inter-particle resistances, but so far with only gross approximations, e.g. with the simplifying assumption of uniform tunneling thickness [13-16]. (To accommodate 1nm variations in a 1-10nm tunneling separation range between particles requires an underlying simulation grid with a 1nm pitch in a brute force approach, i.e. a substantial increase in resolution over that otherwise required for micron sized particles. It would be more efficient, however, and just as valid to superimpose the tunnel gap distribution on contacting islands distributed on a coarser grid.) The structural modeling requirements have been outlined above.

Electrical modeling requires the addition of the conduction processes discussed below to each of the elements: intra-particle, inter-particle, and contact, with the structural model itself providing the percolation component. Existing models confirm the effects of surface layering at a qualitative level [15], and size effects [13, 40], i.e. the increase and decrease in effective conductivity respectively for limited ICA sample dimensions parallel and perpendicular to current flow. In particular, the "short sample" percolation threshold is less than the bulk isotropic value, if the dimension parallel to current flow approaches or falls below the percolation "coherence length," as for practical flip-chip bump-to-pad interconnect. As contact separation decreases to filler particle size, (the ACA situation,) the threshold obviously tends to 0%. On the other hand, for a short dimension perpendicular to current flow, as for example in many experimental test "tracks" along a substrate surface, the percolation threshold increases due to the intersection of percolation paths with the surface. So pad-to-pad "contact" structures tend to possess lower resistivities than the nominal bulk value, and "track" configurations higher resistivities. Flake alignment along the surface tends to produce the opposite effects, increasing the number of inter-particle contacts in z-axis current flow, and short-circuiting the isotropic interior of the "track." Figure 10 shows the track conductance variation with thickness. At low thicknesses the track flakes are all layered, but as thickness increases, the proportion of internal disorder increases [41]. Figure 11 shows the resistance of a z-axis contact as it is mechanically thinned. The sharp drop in resistance corresponds to the removal of the aligned surface layer [42].

As models improve, one expects eventual quantitative agreement. It is probably satisfactory to continue to ignore the effect of finite polymer conductivity, but this assumption should be checked for new materials. One prediction of percolation theory which has never been validated in these systems is the frequency dependence of the conductivity in terms of the coherence length [43], which appears to be masked by the particle skin effect (see below.)

It is noted here that there is evidence of percolation chains dropping in and out of the conduction paths during thermal cycling. This effect is demonstrated by reproducible hysteresis in resistance versus temperature plots during thermal cycling of ICA structures where only a limited number of percolation paths are expected to exist, i.e. for very small contact areas. [44]

(2) *Inter-particle conduction* is generally assumed to take place directly from metal to metal, or by tunneling through an insulating layer, whether of intervening polymer or of surface contaminants, or by conduction through a surface oxide film, which for Ag would be a conductive degenerate semiconductor. There is a range of tools available to characterize conduction mechanisms, including frequency effects, non-ohmic high field behavior, temperature dependencies, etc., and the absence of any observation of negative temperature coefficient of resistance (TCR) or non-ohmic behavior is sufficient to eliminate most other conduction mechanisms from contention. Silver is typically tarnished, and presumably would oxidize within the polymer, even if initially "clean," but it is not clear what effect the surface lubricants identified on flake surfaces [45] would have on this process. An XPS surface analysis of the flake surfaces should be

carried out to distinguish between the presence of Ag oxide and the oxygen content of the lubricant and/or polymer residue.

No matter which of the mechanisms apply at the gap itself, the contact area is accepted as being typically small, of diameter, d, 10 nm or less [6]. Clearly there will be some constriction of current flow between particles at the contact, and the Holm theory specifies this contact resistance to be $\rho/2d$ [2]. With the constriction resistance proportional to d^{-1}, and the tunneling or oxide resistances proportional to d^{-2}, one should be able to identify the dominant contribution from a pressure dependence, which has been theoretically matched to experimental data for a d^{-2} dependence, but not for an ICA [46]. The internal pressure exerted by the curing process must be quantified for further progress to be made. Returning to the differences between the contact conduction mechanisms, the TCR will be zero (or slightly negative) for tunneling and positive for the oxide. Unfortunately, it is difficult to find data on the exact electrical properties of the oxide, which are subject to local formation conditions, so it is not known whether the TCR would be less or greater than the metal particle TCR. It would appear from the formula that the constriction resistance would have the same TCR as the metal particles', but the derivation does not include the mean free path reduction which will be associated with contact dimensions less than the bulk value in the particles; this extension to the theory is necessary.

The inter-particle conduction mechanism remains undetermined, and the points made above, which reflect those in the literature, are very general. What is needed is a comprehensive basic study of the metal-polymer interface, to investigate charge transfer and band effects in the polymer(s), time and temperature effects, and how the process proceeds during curing. In addition, actual contact points need to be located and isolated, and the potential distribution plotted across the boundary from one particle to the other. Electrical noise measurements are also often a useful diagnostic tool, and there is noise data in the literature [47, 48], but as is often the case, the interpretation is ambiguous. Wong has studied the role of the flakes' surface lubricant, and has achieved reduction of overall resistance by replacing the traditional stearic acid with shorter chain alternatives [36, 49]. Benson, on the other hand, has shown that the lubricant breaks down during cure, and leaves a carbon residue on the flake surface [50], which is expected to control the inter-particle resistance.

Frequency dependencies are easily determined and can be definitive in the identification of some conduction mechanisms. In the ICA case, ac measurements were expected to short circuit the tunnel gaps between particles, with the corner frequencies providing the means to separate out the particle resistance from the inter-particle gap contribution. The method was validated by ac measurements before cure. Resistivities below the percolation threshold decreased with frequency to limiting values similar to those above it [51]. (This experiment suggests the use of impedance spectroscopy as a manufacturing quality test for ICAs, as for solder paste.) When applied to cured ICAs, however, no such effect was observed (see below), so either there is no tunneling gap (i.e. conducting oxide or metal-metal contact) or the tunnel resistance is just much less than the particle resistance [2, 4].

(3) *Intra-particle resistance* accounts for a substantial proportion of the measured ICA resistance, and in some cases essentially all of it. This conclusion is based on TCR measurements on a variety of commercial ICAs, where the TCR values range downwards from the bulk metallic value, but are always positive [2, 4, 43]. Within the limits of experimental accuracy, the data are consistent with a model of the intra-particle metallic resistance in series with a zero TCR contact resistance, but cannot be totally conclusive (Figure 12). Thermal testing needs to be extended to much lower temperatures to resolve this point.

For ten micron diameter flakes one micron thick, and micron-sized smaller particles, the electron mean free path is not going to be reduced significantly from the bulk value, and no accounting is needed for size effects in the particles. (Note that this would not apply to the nano-particle ICA variant [52].) But the nature of the surface (i.e. rough or smooth for diffuse or specular scattering) could be important for the assessment of mean free path limitation for constriction resistance.

The ac measurements mentioned above were run on the same ICA materials which gave TCRs identical to the bulk value for Ag, and so it is not surprising that the ac characteristics were in total accordance with the predictions of skin effect resistance and inductance for Ag [4]. These experiments should be duplicated for materials with greater inter-particle resistances.

At frequencies where skin effect is dominant, the lower resistance advantage enjoyed by solder disappears, as the effective cross-sectional area shrinks with the skin depth for solder and ICA alike [42].

(4) *Contact resistance* can be isolated from the bulk composite resistivity by the combination of three-terminal measurement with the more common four-terminal; (see below) [26]. It is the contact resistance which has been shown to be the source of electrical reliability problems [53-55]. The oxidation (corrosion) of Cu or the Sn in Sn/Pb contact pads or Pb coatings has been demonstrated, and explains the greater long term stability of noble metal contacts (Au or Pd under thermal cycling and 85/85 stress testing. More recently galvanic corrosion has been identified between dissimilar metals [56, 57]. One would fully expect to see the effects of interfacial diffusion in the longer term (albeit limited by low process temperatures), and the formation of brittle inter-metallics; although these would probably have no discernible effect on mechanical reliability, the electrical impact could be significant, given the limited number of low diameter contact points to the percolation paths. The solution to these problems would be to eliminate the dissimilar materials, and the use of silvered contacts with Ag-based ICAs would seem logical. However, Ag on Cu introduces much the same problems, and requires a barrier layer (of Ni for example.)

The high-frequency ICA data of Li et al [4] have been extended by Wu et al [58] and by Dernevik et al. [59, 60] Li and Wu focused mainly on the MHz region, and Dernevik on the GHz region. Wu reported that ICA joints can change their high frequency properties during bending.

B. Electrical Measurements

Resistivity measurements must be made on genuinely isotropic samples of suitable size, unless size or layering effects are the actual object of the measurement. On the other hand, the interconnect application will actually include both, as described above. So will measurements along a long thin sample, but with the opposite effects [2]. The measurement of small resistances with sufficient sensitivity to detect early corrosion, etc., is difficult and usually accomplished by depositing the long specimen just mentioned or by daisy-chaining multiple interconnect samples. In future, the impedance transformer should see increased application to solve this problem [2].

Printed ICA "tracks" are also commonly used for 4-terminal and 3-terminal measurements (Figure 13) which provide separation of bulk and contact resistances, an essential step to interpretation of any resistance data. Finite geometries can lead to errors, however, if care is not exercised (Figure 14.) The same sort of problem can be experienced with z-axis samples (and with ACA testing) due to finite track resistances comparable to the sample's (Figure 15) [42]. However, self-consistent results have been demonstrated [61].

C. ACA

We move now to conduction through an individual particle between two contact pads.

The electrical conductivity in an ACA joint has been estimated by Williams et al [23]. Assuming both hard and soft spheres, plastic deforming lands and spheres, the joint contact resistivity (ρ) has been estimated as:

$$\rho = \frac{A\rho_B\left(\sqrt{\frac{6\pi n\kappa}{\sigma A}} - \frac{1}{R_B}\right)}{4\pi n R_B} \qquad (17)$$

for a single particle, where ρ_B is the resistivity of the sphere material, n is the number of contacts within the contact area A, κ is the shear yield stress on a single contact sphere of radius R_B, and σ is the pressure applied to the joint. Using equation (7) one can calculate the electrical conductivity through an ACA joint. For instance, for 25 micron radius Ni alloy particles with $A = 0.1\text{mm}^2$, $\kappa = 1\text{GPa}$, $\rho_B = 6.1 \times 10^{-8}\Omega\text{m}$ and $\sigma = 1\text{MPa}$ we obtain joint conductivity of $4 \times 10^5 \Omega^{-1}\text{m}^{-1}$ with 50 conducting particles and $1 \times 10^5\ \Omega^{-1}\text{m}^{-1}$ for 2 particles.

Shi et al [25] have calculated the resistance of a solid spherical contact particle analytically as the sum of the bulk resistance and constriction resistance components, and then extended the result to include distributed particle sizes and the influence of pressure on the particle contact area. Both elastic and plastic deformation models were included. Yim and Paik [62] also developed an analytical model, but also, like Oguibe et al [63], performed finite element modeling of both solid sphere and coated polymer particle systems. There is direct comparison with experiment and good agreement is claimed. Meanwhile, Fu et al have found that the particle location in an ACA joint can affect the electrical conductivity [64]. Generally speaking, a particle in the center of the joint contributes much more to the electrical performance than a

particle close to the edge of the joint, which helps to explain the large scatter observed in single joint resistance values.

The high frequency properties of ACAs in packaging have also been studied by several groups [65-67]. ACA can offer similar high frequency flip-chip packaging performance up to 20 GHz [65] as solder. Significant transmission loss is due to the silicon material itself. It is characteristic of experimentalcomparisons of ECA joints with solder at high frequencies that the results owe more to the board lines and connections than to either the solder or ACA joints, which both contribute comparably negligible loss to the overall system. Kim [66] has used electrical equivalent circuit modelling of the ACA flip-chip interconnect in conjunction with experiments to extract the high frequency effect of the ACA interconnecting material itself. Fu et al [67] used a physical modelling approach to understand the high frequency performance of the ACA joint. They found that at extremely high frequency, the capacitive displacement bypasses the filler contacts, and the high frequency performance is largely independent of the particle size and number. It is therefore doubtful if arrayed structures can improve high frequencyACF performance.

V. Mechanical Properties

A. ICA

The vast majority of the published ICA data is comprised of electrical resistance and adhesive strength measurements, both presented in the context of reliability testing. But while there has been some parallel effort to interpret the electrical properties in terms of both structure related and physical failure models, there has been little similar effort to understand the mechanisms of adhesion at a comparably fundamental level. Obviously, such a study requires a systematic approach to the measurement of adhesive strengths for a matrix of metal surface and polymer combinations. It is clear that surface cleanliness plays a crucial role in effective adhesion, (and one which may be overlooked in the desire to apply ICAs as drop-in replacements for solder), so surface treatments must be included as a secondary variable, with consideration of roughening effects also included. While this could be regarded as an empirical study, the fundamental goal of determining the relative contributions of various adhesion mechanisms (e.g. chemical, mechanical, electrical) should not be lost sight of.

Plasma cleaning of the adherent surfaces would seem to be a logical step, but so far preliminary data shows no improvement in adhesive strength with either Ar or O_2 plasma treatments, despite the demonstrated removal of organic contaminants and oxides [12, 59]. Wolter et al [68, 69] have demonstrated that it is the polar component of surface energy which is increased by plasma treatments. Experimental studies consistently show that the mechanical component of adhesion dominates [70-71], with best results from surface roughening, (which may be accomplished by high energy plasmas.) (A simple NCA shows good electrical stability, provided the contact surfaces are roughened [41].)

Published ICA adhesive and shear strengths are on the same order as those of solder, usually a little less [72], occasionally higher [69], but anyway adequate. The problem has been the drop test failure rate, leading to the widespread adoption of the NCMS criteria [73] as a de facto standard. In general, it is the larger devices which are most at risk, and indeed current commercial materials seem adequate for smaller devices such as SMT passives, which have been in mass production with ICA attachment for some years, e.g. in automotive electronics. Improved understanding of this particular phenomenon is currently leading to the development of ICA materials specifically designed to address the drop test problem. The key lies in the imaginary component of the complex Young's modulus, which represents energy dissipation in the material, as opposed to the energy storage of the simple deformation represented by the conventional form of Hooke's Law. The complex modulus is therefore directly analogous to the complex dielectric constant, and dynamic stress-strain relationship actually includes a phase shift. When one examines drop test survival data, the success rate correlates with the (imaginary) dissipation modulus rather than with adhesive strength [74, 75]. One way to design materials with high dissipation modulus is to select polymers with glass transition temperature T_g below the operating range, i.e. below room temperature, in general [76]. However, operating polymers above T_g carries its own penalties, e.g. higher temperature coefficients of expansion, so the next step is to develop adhesive polymer blends with high mechanical absorption without those disadvantages.

Figure 16 shows the improvement in drop test results for a commercial ICA with the addition of a pre-cure heat soak to the processing schedule [77]. The additional step enables the material to survive an

additional 20 4-foot drops and at least 10 more from 5 feet, greatly exceeding the NSMC standard. Improvement in resistance, adhesion, and drop test results are all tentatively attributed to the elimination of bubbles at the contact interfaces, where they reduce the effective contact area.

B. ACA

Several research groups have now studied the deformation effect on the electrical conduction development during the ACA assembly [62, 64, 78, 79]. The key work has been done by Wu et al [78] where they consider two types of particle situations as shown in Figure 17 (rigid and hard particle) and in Figure 18 (soft particle).

In addition, Wu et al have also successfully deduced an equation that describes the relationship between the resistance and bonding pressure. These are shown in Figure 19 and 20 for the rigid and deformable particles respectively.

Wang et al also focused on quantification of criteria for a good ACA flip-chip joint, as this is one of the most important issues during the ACA bonding process [80]. The purpose of their work was to study the relationship between bonding pressure and the deformation of conducting particles in ACAs. It has been shown that the deformation of filler particles plays an important role in both bonding quality and the reliability of ACA joints. The deformation degree as a function of bonding pressure during ACA film flip-chip bonding is shown in Figure 21. As can be seen, deformation and bonding pressure exhibit a linear relationship.

As the mechanical properties of a thin layer adhesive material differs from its bulk material properties, it is important to know the ACA material properties for mechanical model and simulation purposes. Because of this, Young's modulus and Poisson's ratio have been determined by Zribi et al [81] for an ACF over the temperature range of 15 to 60°C (Figure 22.)

A Chalmers group has recently carried out theoretical simulation in order to explain the microscopic mechanism of the electrical contact conduction through the metal fillers for ACAs. By comparing with experiments performed at Wang et al [80], it was concluded that the deformation of the metal filler is plastic even at rather low external loads. Further theoretical simulation reveals two aspects of the conductance characteristics: the conductance is improved by increasing the external load, but the dependence of the conductance becomes stronger on the spatial position of the metal filler [65].

The consequence of the bonding pressure during the ACA bonding on the stress generation is evident. This stress generation is probably the reason for catastrophic failure. Wu et al have simulated this using finite element modelling. They have found that both for rigid and deformable particles, significant stress is built up in the interface between the two contacts [78]. Wang et al used a similar approach to calculate the stress after various degrees of deformation [65, 69]. It is clearly shown in Figure 23 that the highest stress point is in the edge of the ACA particle.

Lai et al have proposed a similar failure mechanism of the ACA flip-chip joint structure [82] as can be seen in Figure 24(a). In this case, the particles are exposed to large shear stress due to the expansion of the substrate. Therefore, it seems that the stress concentration is the most critical parameter that governs the reliability of the ACA joint. Therefore the failure mechanism of ACA joint differs from the traditional solder joint failure mechanism where plastic strain is the most critical parameter that governs the joint reliability, see Figure 24(b0.

A most complete ACA joint stress analysis has been done by Wu et al [83]. It is shown that the residual stress is larger on a rigid substrate than on a flexible substrate after bonding.

As an ACA bonded module may be used in connection with soldering technology for a final product, we need to know if the ACA material can withstand the soldering temperature. Sugiyama et al reported that the ACA material from Sony can withstand the soldering profile three times and without causing reliability problems [84]. Törnvall reported different results in terms of soldering effect where he showed that an ACA flip-chip module cannot withstand a normal soldering process [85]. More research is therefore needed to clarify this matter further.

Oxidation is an ACA joint failure mechanism that was identified at an early stage [86]. The idea was that the particle is oxidised causing electrical performance decrease. For a parabolic oxide growth law, and assuming the resistance change, ΔR, is ohmic, then the change with time, t, is given for contact area, A, by

$$\Delta R = (2Dt)^{1/2} \rho_{oxide} / A \qquad (18)$$

where D is the diffusion constant of oxygen in the metal filler, and ρ_{oxide} is the volume resistivity of the oxide.

VI. Thermal Properties

A. Thermal Characteristics

The thermal performance of an adhesively assembled chip is of vital interest as power dissipation in the chip increases. Power dissipations have been simulated by Sihlbom et al for both ICA and ACA flip-chip joints [87]. They concluded that the ACA flip-chip joint is more effective in transferring heat to the substrate from the powered chip than the ICA joint, because the adhesive thickness is so much thinner than the ICA joint.

B. Maximum Current Carrying Capacity

Dernvik et al have also studied the effect of maximum current carrying transmission capacity through the ACA adhesive joints at 3.2GHz [59]. The copper bridge structure was subjected to a maximum transmission of 25W of average pulsed power for 10 minutes, with a pulse length of 10μs and peak power of 250W at duty cycles of 1, 5 and 10%. The result indicated that bonding pressure has a strong influence of the joint quality. At 150 N, no electrical transmission loss is observed, but for 75N bonding force, some deterioration was observed after the final power exposure; however, the effect was small, at about 0.5dB.

In a similar dc study of three ICAs, Morris et al [12] found that failure correlated directly with temperature rise, which in turn correlated with the joint resistance, and hence to power dissipation. The breakdown mechanism was clearly polymer degradation, accompanied by the emission of noxious fumes. The onset of breakdown shows thermal runaway, (Figure 25,) as measured at the adhesive surface. Comparisons of surface temperatures with estimates of internal temperatures, (from resistance values and the previously measured temperature coefficient of resistance (TCR),) suggest that the internal temperature at this point is a good 60-80°C higher than the 200°C shown. While two of the ICAs failed like this at 9A/mm^2, the other showed no ill effects whatsoever.

Bauer et al has studied the power dissipation performance of NCA joints under dc conditions. It was found that the NCA joints still show ohmic behavior up to 25 A/mm^2 [88].

VII. Reliability

A. ICA

(1) *Cure schedule* control is undoubtedly very important for joint reliability. It seems that the electrical resistance of the joint is related to the curing degree, especially for non-noble metal surfaces, as can be seen in Figure 26. Figure 26(a) shows the contact resistance vs. curing time for an epoxy conductive adhesive cured at 150^{0}C, and following 1000 hours of damp heat treatment at 85^{0}C, 85%RH [89]. The corresponding curing degree varies between 65% and 90%, determined by DSC. Below a critical curing degree, (77% for this adhesive,) the electrical resistance of the joint increases significantly, because an incompletely cured epoxy can absorb a significant amount of moisture, which in turn causes oxidation/hydration of the Sn37Pb bonding surface in Figure 26(a) [90]. If a noble metal, for instance Au or Pd is used as the bonding surface, no electrical resistance change is observed, despite the fact that the curing degree can be very low, (Figure 26(b).) Once a critical curing degree is reached (72%), it seems that the shear strength of the joint on the Sn37Pb bonding surface can be maintained at a constant level as is illustrated in Figure 27(a). However, on the noble metal bonding surface, the shear strength of the joint is almost independent on the curing degree in the range from 67% to 92%, (Figure 27(b).) In summary, it can be said that a minimum curing degree appears to be required to provide a certain level of mechanical and electrical performance in the adhesive system. Once this is achieved, increasing curing times do not result in significant improvement. At full cure conditions, however, the electrical resistance and the mechanical strength of conductive adhesives are also guaranteed [91]. These above results also indicate that for conductive adhesive joining, noble metal surfaces are preferred to non-noble metal surface.

(2) *Moisture effects* on the polymer degradation in conductive adhesives have been studied by Khoo and Liu [92]. Moisture sorption effects may be reversible or irreversible, and are usually small enough to make detection of the molecular changes during absorption/adsorption very difficult. Figure 28(i) shows the FTIR spectra of an ACA (but ICAs would be similar) after curing and subsequent 41 hours conditioning at 85°C and 85%RH. The difference spectrum (a)-(b) in represents the changes occurring due solely to

exposure to the moisture conditions at 85°C and 85% RH. The most obvious real changes are the negative bands at 868, 916, 1345, 3005 and 3058cm^{-1}, implying decreasing epoxy functionality, and thus further progress of the cure reaction. The new bands at 3560 and 3350cm^{-1} may both be attributed to hydroxyl groups, of which the former are free groups, which could be formed on further curing, or as an oxidation product resulting from thermo-oxidation/degradation processes. The latter are attributed to hydrogen-bonded hydroxyl groups, indicating the type of bonding of the adsorbed water to the epoxy resin. The slight rise at about 1640cm^{-1} indicates the presence of absorbed water in the epoxy resin. Finally, new ester linkages indicative again of further curing are indicated by the presence of a broad absorption region between 1000 and 1300cm^{-1}.

Figure 28(ii) compares the molecular events happening on further exposure to these same conditions. The figure shows the difference spectra (a) after 41 hours conditioning, (b) after 162 hours conditioning, (c) after 821 hours conditioning, all at 85°C and 85% RH. It is observed firstly that the subtracted spectra all show the same profile, indicating that the subtraction procedure has been consistent and that the subtraction spectra are valid, but a closer scrutiny also shows that the bands at 3560, 3350, 1640, 1573cm^{-1} are increasing in intensity with increasing conditioning time. Both the increases at 3350 and 1640cm^{-1} follow the increasing adsorption of water in the epoxy. The steadily growing absorption at 1573cm^{-1} is tentatively attributed to unsaturated vinyl structures ("C=C") which are formed as a result of degradation actions. Moisture degradation is felt to occur by hydrolysis of the ester linkages ("R-(C=O)-OR'). Such hydrolytic attack breaks the polymer chain creating two new end groups, a hydroxyl and a carbonyl. Although it is difficult to see a new emerging carbonyl group in this figure, the presence of the band at 3560cm^{-1}, which indicates free hydroxyls, supports the suggestion of degradation reactions occurring with increasing exposure to heat and humidity at 85°C and 85% RH. Hence, in conclusion, it can be said that on exposure of the cured adhesive to 85°C and 85% RH, both moisture adsorption and further curing can be observed. After a certain time, however, further curing will not be observed, but instead, degradation effects may be seen.

(3) *Galvanic corrosion* at the contact interfaces has been demonstrated by Lu et al [56, 57]. They correlated the degree of contact corrosion (as indicated by resistance increases) to the electrochemical series, and demonstrated the requirement for moisture in the process. With this understanding of the process, it was shown that resistance drift could be inhibited by the addition of corrosion inhibitors, oxygen scavengers, and/or sacrificial anode material to the polymer matrix [93-95]. Figure 29 illustrates the classic result. The bulk ICA resistance varies little, decreasing somewhat with further cure. The contact resistance changes little for the Ag filler on a Au surface, but corrosion produces major increases for the Ag/Cu combination.

(4) *Thermomechanical* cycling is the litmus test for all package interconnect, especially for soldered flip-chip, and there are many examples of ICA data in the literature. Polymer cure temperatures are usually less than even the lowest solder reflow temperatures, so initial thermomechanical stress is lower at room temperature. In addition, the ICA's polymer base provides greatly increased creep properties in comparison to its solder competitors [96], so it may relax more readily to a zero stress state. It is therefore not surprising that ICAs out-perform solder on mechanical cycling tests by an order of magnitude, (Figure 30) [97]. In an SMT application, however, the thermoplastic properties of the polymer lead to the accumulation of plastic strain, which initiates cracking [29].

B. ACA

The bonding pressure, if not homogeneously distributed, can cause uneven deformation of the particles. There are many possible reasons for uneven pressures, but the main reasons are improper electrical routing on the substrate, un-adjusted pressure bonding head, etc. It is also clear that on rigid and thick substrates, electrical routing is not so critical, but it is crucial on thin and flexible circuitry.

Electrical failures during thermal cycling are observed at both low and high temperatures, and the different types of failure (Figure 31) can be attributed to different combinations of particle size and chip geometry, as can be seen in Figure 32, [98]. The best case is that the particles are deformed uniformly and atomic bonding between the particles and contacts is achieved (type I). If the particles are just in contact with the bonding surface, we will have a situation that electrical reliability is not good at high temperature due to the fact that epoxy will expand more than the metal particles (type II). If the particles are not the same in size and for unbumped dies and for chips with non-uniform bump heights, one obtains a situation that the smaller particles are not deformed and will shrink more than the big particles causing problems at

low temperature (Type III). The final case is when there is a uniform height of the bump and chip surface but very a large particle size variation. This will cause electrical opens at both low and high temperature (Type IV).

The dynamic pressure on the particle necessary to cause separation from the contact is, for the deformed (polymer particle) case, given by [98]:

$$P_i = N\left(\frac{1}{b^2}\right)\sqrt{\frac{\rho}{AB}}\frac{1}{\cos\alpha} \qquad (19)$$

where P_i is the stress necessary for decohesion, N is the bonding force, ρ is the curvature of the particle , b, l and AB are geometric length, and α is the decohesion angle. For the undeformed (Ni sphere) case, a similar equation can be obtained [98]:

$$P'_i = N'\left(\frac{1}{b^2}\right)\sqrt{\frac{\rho'}{A'B'}}\frac{1}{\cos\alpha'} \qquad (20)$$

From equations 19 and 20 it is clearly seen that $P_i > P'_i$. Therefore, for the deformed case, a larger stress is necessary to cause decohesion and, for the same stress level, it is easier to obtain failure with an undeformed particle.

As shown analytically by Hu et al, the electrical resistance decreases with increasing bonding pressure, until the polymer coating fractures. This has been demonstrated experimentally [14, 99].

Another important issue is the substrate hardness, geometry and material. A soft substrate material may deform during the bonding due to the softening of epoxy at the bonding temperature, which is above the glass transition temperature (T_g) of the epoxy matrix. On an FR-4 substrate, it has been observed that the electrical conductivity and reliability of a joint depends on the depth of the glass fibre in the substrate where the bump exerts pressure on the pad [100]. Deeper fibres mean thicker layers of soft epoxy that deform more readily during the bonding. Therefore, insufficient particle deformation will be obtained at that point. Shorter distances to the fibre bundles resist substrate deformation better, and hence yield better electrical conductivity and reliability. See Figures 33 and 34. One approach to reduce the amount the pad can sink into the substrate is to use a relatively large pad area in comparison to the bump area to reduce the pad pressure for a given bonding force.

Despite the complex processing and manufacturing conditions, under optimum conditions, good reliability data on ACA flip-chip joint has been reported [101]. Cumulative fails after the temperature cycling test from -40 to $+125^0$C for 3000 cycles with a hold time of 15 minutes at hold temperature are shown in Figure 35. However, the number of fails is dependent on the definition of the failure. Figure 35 shows three interpretations of the same cumulative failure data, based respectively on the different criteria: >20% of contact resistance increase; >50 mΩ; >100mΩ. When the criterion was defined at 20% of resistance increase, all joints failed after 2000 cycles. This definition might be too harsh for those joints having initial contact resistances of only several mΩ. The 20% increase means only variations of a few milliohms are allowed. In some cases, the limitation is still within the margin of error of the measurement. Therefore, it is reasonable that the criterion be defined according to the production requirements. However, if we define failure as 50 or 100 mΩ, the mean times between failures (MTBF) become 2500 and 3100 cycles respectively.

In order to predict the real service life under different environmental conditions, a low-cycle fatigue testing machine was used to perform low-cycle fatigue experiments on ACA made joints in both dry and humid environments at different temperatures [81]. The final goal was to predict the real service life using the fatigue life data generated under different plastic strain loads. The plastic strain is a function of the temperature cycling interval, frequency and temperature ramp rate etc. The daisy chain resistance curves versus the number of cycles are shown in Figure 36. A fairly significant decrease of the load level was noticed during the test. The load level ranged for both samples between 1N and 0.7N. According to the test data, failure occurred in the humid environment much faster than in the dry environment, which was physically expected. In fact in the humid atmosphere, the joints are subjected to very severe operating conditions (expansion of the adhesive due to moisture uptake, creep of the adhesive under exhaustive conditions).

There are two features of ACA flip-chip joining technology, which are different from other microelectronic interconnection techniques, such as flip-chip soldering, surface mounting etc. These are:

- Application of bonding force
- Simultaneous bonding of all bumps of a chip

As the conductivity of ACA joints is directly determined by the mechanical contact between the terminals of chips and the electrodes on chip carriers, the bonding force plays a critical role in the electric performance. High bonding pressure is certainly favorable to an intimate contact, and thus to a low contact resistance. In addition, because the bonding of all bumps of a chip is performed simultaneously, uniform conductivity of all joints in the chip requires the bonding situation of every joint to be completely the same. In other words, every joint in the chip must have:

- Same bonding pressure
- Same number of conducting particles
- Same particle size
- Same bump and pad geometry

In practice, these requirements are hardly ever met. Many factors can affect the bonding situation, including:

- Distribution of bonding pressure on bonding tool
- Alignment
- Variation of conductive particle size
- Distribution of particles in bonding area
- Pad planarity
- Bump planarity
- Variation of substrate thickness

Although we understand significant amount of the ACA joining technology, we still need to understand the following issues:

- High frequency behaviour, its coupling with semiconductor devices, cross-talk between the particles especially at the range beyond 20 GHz.
- The maximum current carrying capability at high frequency and also after exposure to various environmental tests.
- The planarity effect of the substrate on the ACA joint reliability. This remains one of the most important issues to be understood before we can use ACA in real high volume for low-cost applications.
- Life time prediction models of ACA joints. For this, we need to understand further the effect of UV-degradation of the polymer chain, the corrosive gas effect and high temperature storage effect.

C. General Comments

As conductive adhesives are made of polymers and metal fillers, light may break the polymer chain. How this works is still unclear as there is no report on this work.

A similar situation is noted as to how various gases affect the polymer chain stability in conductive adhesive applications, although it is clear that polymer chains may be affected and broken by the corrosive gases.

One of the major important questions that need to be addressed is the estimation and prediction of the real service life of a conductive adhesive joint. As conductive adhesives consist of a metal part and an epoxy part, it is a composite material. Therefore, it is unlikely that the acceleration laws used for prediction of the real service lives of pure metals and pure polymers can be directly used for conductive adhesives.

VIII. Environmental Impact

The environmental impact of ECAs has been studied by several research groups [102-104]. Segerberg et al [103] compared use of conductive adhesive joining with soldering for SMT applications and concluded that it is really dependent on the mining condition of silver when determining the environmental load of the conductive adhesives. If silver is mined in a silver mine, then the environmental load is much smaller compared to soldering. On the other hand, if it is mined as a by-product in a copper mine, then conductive adhesive joining technology will have a much larger environmental load index compared to soldering.

Westphal et al [102] came to the conclusion in their study that conductive adhesives are generally better in terms of environmental loading compared to solder. More work is needed to clarify this topic.

IX. Further Study

Readers are directed to references [105] and [106] for introductory concepts and a more comprehensive coverage respectively. Recent reviews of ACAs include references [107, 108.] In addition, many of the points made here are expanded on in the on-line course at www.cpmt.org [109]. This work has been an update of an earlier review [110.]

X. References

1. J. Kivilahti (personal communication)
2. J. E. Morris in "Electrically Conductive Adhesives: A Comprehensive Review" J. Liu editor, Electrochemical Press, UK, (1999) 37-77.
3. R.P.Kusy, J. Appl. Phys. 48 5301-5305 (1977)
4. Li Li, H. Kim, C. Lizzul, I. Sacolick, & J. E. Morris, IEEE Trans. CPMT 16 (1993) 843-851.
5. Ying Fu, Johan Liu and Magnus Willander, International Journal of Adhesion and Adhesives.
6. Li Li, Ph.D. dissertation, State University of New York at Binghamton, 1995.
7. J. Constable, T. Kache, S. Muehle, H. Teichmann, & M. Gaynes, IEEE Trans. CPT 22(2) June 1999, 191-199.
8. P. Li, E. Cotts, Y. Guo & G. Lehmann, Proc. 3rd International Conference on Adhesive Joining & Coating Technology in Electronics Manufacturing, Binghamton NY, Sept., 1998 (Adhesives'98), pp. 328-333.
9. M. Mundlein & J. Nicolics, Proc. 4th International Confer. Polymers & Adhesives in Microelectronics & Photonics, Portland, Oregon, 2004, PP-3.
10. E. Sancaktar & N. Dilsiz, J. Adhesion Sci. & Technol., 10 (1996).
11. T. Inada & C.P.Wong, Proc. 3rd International Conference on Adhesive Joining & Coating Technology in Electronics Manufacturing, Binghamton NY, Sept., 1998 (Adhesives'98), 156-159.
12. J. E. Morris, C. Cook, M. Armann, A. Kleye, & P. Fruehauf, Proc. 2nd International Symposium Polymeric Electronics Packaging (PEP'99), Gothenburg, Sweden, 1999, pp. 15-25.
13. E.Sancaktar & N.Dilsiz, Proc. 3rd International Conference on Adhesive Joining & Coating Technology in Electronics Manufacturing, Binghamton NY, Sept., 1998 (Adhesives'98),, 90-95.
14. Li Li & J. E. Morris, J. Electronics Manuf. 5(4) Jan 1996, pp.289-298.
15. Li Li & J. E. Morris, IEEE Trans. CPMT:A-20(1). March 1997, pp. 3-8.
16. P. McCluskey, J. E. Morris, V. Verneker, P. Kondracki, & D. Finello, Proc. 3rd International Conference on Adhesive Joining & Coating Technology in Electronics Manufacturing, Binghamton NY, Sept., 1998 (Adhesives'98), 84-89.
17. Mustoe, G. G. W., Nakagawa, M., Lin, X., & Iwamoto, N., Proc. 49th IEEE ECTC, San Diego, (1999).
18. M. Mundlein, G. Hanreich, & J. Nicolics, Proc. 2nd International IEEE Confer. Polymers & Adhesives in Microelectronics & Photonics (Polytronic 2002), Zalaegerszeg, Hungary, pp. 68-72.
19. L. Li & J. E. Morris, Proc. Adhesives'94, Berlin, 1994.
20. A. O. Ogunjimi, S. H. Mannan, D. C. Whalley & D. J. Williams, Adhesives in Electronics '96, 270-284
21. Williams, D.J. and Whalley, D.C. (1993), , Journal of Electronics Manufacturing, Vol.3, pp85-94 .
22. Herczynski, R. (1975), Nature, Vol. 255, pp. 540-541.
23. Williams, D.J., Whalley, D.C., Boyle, O.A. and Ogunjimi, A.O. (1993), Soldering & Surface Mount Technology, No.14, pp. 4-8.
24. Mannan, S.H., Williams, D.J., Whalley, D.C. and Ogunjimi, A.O. (1999), in Conductive Adhesives for Electronics Packaging, edited by Johan Liu, Electrochemical Publications Ltd, 1998.
25. F. Shi, M. Abdulla, S. Chungpaiboonpatana, K. Okuyama, C. Davidson, & J. Adams, Proc. 4th International Symposium Advanced Packaging Materials, Braselton, GA, 1998, pp. 163-168.
26. D. Klosterman, L. Li, & J. E. Morris, IEEE Trans. CPMT Part A, 21(1) March 1998, 23-31.
27. L.Li & J.E.Morris, "Electrically Conductive Adhesives: A Comprehensive Review" J. Liu editor, Electrochemical Press, UK, (1999) 99-116.
28. J. E. Morris & S. Probsthain, Proc. Adhesives in Electronics 2000, Espoo, pp. 41-45.

29. M. G. Perichaud, J. Y. Deletage, D. Carboni, H. Fremont, Y. Danto, & C. Faure, Proc. 3rd International Conference on Adhesive Joining & Coating Technology in Electronics Manufacturing, Binghamton NY, Sept., 1998 (Adhesives'98), pp. 55-61.
30. O. Rusanen & J. Laitinen, Proc. 4th International Confer. Polymers & Adhesives in Microelectronics & Photonics, Portland, Oregon, 2004, AP2-4.
31. Y.Wei, Ph.D. dissertation, Clarkson University, 1995.
32. J. E. Morris & J. H. Das in "Electronics Packaging Forum, Vol. 3," J. E. Morris (ed) IEEE Press (1994) 41-71.
33. J. E. Morris & J. Das, IEEE Trans. CPMT-B:Adv. Pkg. 17 (1994) 620-625.
34. E. Sencaktar, P. Rajput, & A. Khanolkar, Proc. 4th International Confer. Polymers & Adhesives in Microelectronics & Photonics, Portland, Oregon, 2004, RT2-1.
35. K-S. Moon, J. Wu, & C-P. Wong, IEEE Trans. CPT 26(2) June 2003, pp. 375-381.
36. C-P. Wong & Y. Li, Proc. 4th International Confer. Polymers & Adhesives in Microelectronics & Photonics, Portland, Oregon, 2004, PL-1.
37. K. Suzuki, Y. Shirai, N. Mizumura, & M. Konagata, Proc. 4th International Confer. Polymers & Adhesives in Microelectronics & Photonics, Portland, Oregon, 2004, MP3-1.
38. Samjid Mannan, David Williams, David Whalley and Adebayo Ogunjimi, in "Conductive Adhesives for Electronics Packaging," edited by Johan Liu, Electrochemical Publications Ltd, UK, pp 78-98, 1998.
39. P.Smilauer, Contemp. Phys. 32 89-102, 1991
40. G. R. Ruschau, S. Yoshikawa, & R. E. Newnham, Proc. 42nd ECTC, May 1992, Atlanta GA, 481-
41. J. E. Morris, F. Anderssohn, E. Loos, & J. Liu, Proc. 26th Internation al Spring Seminar on Electronics Technology, Stara, Lesna, Slovak Republic, 2003, pp. 90-94.
42. J. E. Morris, F. Anderssohn, S. Kudtarkar, & E. Loos, Proc. 1st International Confer. Polymers & Adhesives in Microelectronics & Photonics, 2001, Potsdam, Germany, pp. 61-69.
43. R. Zallen, "The Physics of Amorphous Solids," Chapter 4, Wiley, New York, 1983.
44. J. E. Morris, S. Youssof, & X. Feng, J. Electronics Manuf. 6(3) Sept 1996, pp.219-230.
45. C. P. Wong, D. Lu & Q. Tong, Proc. 3rd International Conference on Adhesive Joining & Coating Technology in Electronics Manufacturing, Binghamton NY, Sept., 1998 (Adhesives'98),, 184-192
46. E.Sancaktar & N.Dilsiz, Proc. 3rd International Conference on Adhesive Joining & Coating Technology in Electronics Manufacturing, Binghamton NY, Sept., 1998 (Adhesives'98),, 334-344
47. U. Behner, R. Haug, R. Schutz & H. L. Hartnagel, PEP'97, 243-248.
48. l. Vandamme, M. Perichaud, E. Noguera, Y. Danto, & U. Buehner, IEEE Trans. CPT 22(3) 1999, pp. 446-454.
49. Y. Li, K. Moon, H. Li, & C-P. Wong, Proc. 6th IEEE CPMT Confer. High Density Microsystem Design & Packaging & Component Failure Analysis (HDP'04), Shanghai, 2004, pp. 236-241.
50. J. Miragliotta, R. C. Benson, & T.E. Phillips, Proc 8th International Symposium Advanced Packaging materials, Atlanta, GA, 2002, pp. 132-138.
51. H. Kim, unpublished data (1992).
52. S. Kottaus, R. Haug, H. Schaefer, & B. Guenther, and B. Guenther & H. Schaefer, Adhesives in Electronics '96, 14-17 & 55-59.
53. J. Liu, K. Gustafsson, Z. Lai & C. Li, Adhesives in Electronics '96, 141-153
54. Li Li, J. E. Morris, J. Liu, Z. Lai, L. Ljungkrona, & C. Li, Proc. 45th ECTC, Las Vegas, NV, May 1995, 114-120.
55. H. Botter, R. B. Van Der Plas & A. A. Junai, Int. J. Microelec. Pkg, 1(3) 1998, 177-186.
56. D. Lu, C. P. Wong & Q. K. Tong, 49th ECTC, San Diego, June 1999.
57. D. Lu & C-P. Wong, Proc. 2nd International Symposium Polymeric Electronics Packaging (PEP'99), Gothenburg, Sweden, 1999, pp. 1-8.
58. Sean Wu, Kai Hu, Chao-Pin Yeh, in "Conductive Adhesives for Electronics Packaging," edited by Johan Liu, Electrochemical Publications Ltd, UK, pp117-150, 1998.
59. M. Dernevik, R. Sihlbom, Z. Lai, P. Starski, and J. Liu, Pacific Rim/ASME International Intersociety Electronic and Photonic Packaging Conference, Kohala Coast, Hawaii, 1997.
60. R. Sihlbom, M. Dernevik, Z. Lai, P. Starski, and J. Liu, Polymeric Electronics Packaging, Norrköping, Sweden, 1997.
61. A. Kulkarni & J. Morris, Proc. 3rd International IEEE Conference Polymers & Adhesives in Microelectronics & Photonics, Montreux, Switzerland, 2003, pp. 333-336.

62. Yim, M.J. and Paik, K.W, (1998), IEEE CPMT Transactions, Part A, Vol. 21, No 2. pp 226-234.
63. C. Oguibe, S. Mannan, D. Whalley, & D. Williams, IEEE Trans. CPMT-A 21(2) 1998, pp. 235-242.
64. Fu, Y., Wang, Y.L., Wang, X., Liu, J., Lai, Z. and Chen G. L. and Willander, M. (2000), IEEE CPMT transactions, Part B: Advanced Packaging, Vol.23, No 1, pp. 15-21.
65. Sihlbom, R., Dernevik, M., Lindgren, M., Starski, P., Lai, Z. and Liu, J., IEEE CPMT Transactions Part A, Vol. 21, No 3, pp478-492.
66. Kim, J, (2000), Proc. 2nd International Academic Conference, March 17-19, Atlanta, USA.
67. Fu, Y., Liu, J. and Willander, M. (1999), Journal of Electronics Manufacturing, Vol.9, No 4, pp.275-281.
68. A. Paproth, K-J. Wolter, T. Herzog, & T. Zerna, Proc. 24th International Spring Seminar Electronics Technology, Romania, 2001, pp. 37-41.
69. T. Herzog, M. Koehler, & K-J. Wolter, Proc. 2004 Electronic Components & technology Confer., Las Vegas, pp. 1136-1141.
70. S. Liong, C-P. Wong, & W. F. Burgoyne, Jr., Proc. 8th International Symposium on Advanced Packaging Materials, Braselton, GA, 2002, pp. 260-270.
71. L. L. W. Chow, J. Li, & M. M. F. Yuen, Proc. 8th International Symposium on Advanced Packaging Materials, Braselton, GA, 2002, pp. 127-131.
72. R.Luchs, Adhesives in Electronics '96, 76-83
73. M. Zwolinski, J. Hickman, H. Rubin, Y. Zaks, S. McCarthy, T. Hanlon, P. Arrowsmith, A. Chaudhuri, R. Hermansen, S. Lau & D. Napp, Adhesives in Electronics '96, 333-340.
74. Q. Tong, S. Vona, R. Kuder & D. Shenfield, Proc. 3rd International Conference on Adhesive Joining & Coating Technology in Electronics Manufacturing, Binghamton NY, Sept., 1998 (Adhesives'98) 272-277
75. Q. Tong, C P Wong et al, Proc. 4th International Symposium and Exhibition on Advanced Packaging Materials, Processes, Properties and Interfaces, Braselton, Georgia, 1998.
76. S. Luo & C-P. Wong, Proc. 8th International Symposium on Advanced Packaging Materials, Braselton, GA, 2002, pp. 226-231.
77. S.A. Kudtarkar & J. E. Morris, Proc. 8th International Symposium on Advanced Packaging Materials, Braselton, GA, 2002, pp. 144-150.
78. Wu, S., Hu, K.X. and Yeh, C. P., (1999), in Conductive Adhesives for Electronics Packaging, edited by Johan Liu, Electrochemical Publications Ltd, 1998.
79. Wang, Y.L, Chen, G.L., Liu, J and Lai, Z. (1999), Proc. 2nd IEEE International Symposium on Polymeric Electronics Packaging, Göteborg, Sweden, pp.199-206.
80. Wang, X, Wang, Y. L., Chen, G. L., Liu, J. and Lai, Z. (1998), , IEEE CPMT Transactions Part A, Vol 21, No, 2, pp. 248-251.
81. Anis Zribi, Katrin Persson, Zonghe Lai, Johan Liu, Yilan Kang, Shouwen Yu and Magnus Willander, 2nd International ATW on Flip-Chip Technology, Braselton, Georgia, 1998.
82. Lai,Z, Lai, R.Y, Persson, K. and Liu, J. (1998), Journal of Electronics Manufacturing, Vol. 8(3/4), pp 217-224.
83. Wu, C.M.L. and Liu, J., Yeung,N.H.,(2001), "Reliability of ACF in Flip-Chip with various bump height, Soldering & Surface Mount Technology, 13/1, pp25-30.
84. T. Sugiyama, The latest bare chip bonding by ACF, Sony Chemicals, seminar documentation at Chalmers University of Technology, 2000.
85. Törnvall, M., (2000), Proceedings of a Swedish National Seminar on Environmentally Compatible Materials Research for Electronics Packaging, IVF.
86. J. Liu. and R. Rörgren, Journal of Electronics Manu-facturing, Vol. 3, 1993, pp.205-214.
87. Anders Sihlbom, Rolf Sihlbom and Johan Liu, Electronic Packaging Technology Conference, December 8-10, 1998, Singapore.
88. Andreas Bauer and Thomas Gesang, in "Conductive Adhesives for Electronics Packaging," edited by Johan Liu, Electrochemical Publications Ltd, UK, pp. 313-341, 1998.
89. Cynthia Khoo, Johan Liu, Maria Ågren and Thomas Hjertberg, Proc. 1996 IEPS Conference, Austin, Texas, 1996, pp 483-501.
90. Johan Liu, Katrin Gustafsson, Zonghe Lai and Changhai Li, IEEE Trans. CPMT-A, Vol.20, No1, pp21-30, March 1997.

91. Johan Liu, Pontus Lundström, Katrin Gustafsson and Zonghe Lai, EEP-Vol. 19-1, Advances in Electronics Packaging, 1997 Volume 1 ASME 1997, pp. 193-199.
92. Khoo C. and Liu,J., (1996), Circuit World, Vol.22 No.4, pp. 9-15.
93. Q. K. Tong, D. Markley, G. Fredrickson, & R. Kuder, Proc. 49th ECTC.
94. D. Lu & C-P. Wong, IEEE Trans. CPT 23(4) Dec., 2000, pp. 620-626.
95. H. Takezawa, T. Mitani, T. Kitae, H. Sogo, S. Kobayashi, & Y. Bessho, Proc. 8th International Symposium on Advanced Packaging Materials, Braselton, GA, 2002, pp. 139-143.
96. O. Rusanen, Ph.D. dissertation, University of Oulu, (2000) VTT Publication 407.
97. O. Rusanen, Proc. Adhesives in Electronics 2000, Espoo, Finland, pp. 194 - 198.
98. Lai, Z. and Liu, J.(1996), IEEE Transactions of CPMT, Part B: Advanced Packaging, Vol. 19, No. 3, pp. 644-660.
99. Liu, J. (1999), Advanced Flip-Chip Workshop, March 3-5, Atlanta, USA,
100. Liu, J., Tolvgård, A., Malmodin J. and Lai, Z. (1999), IEEE Transactions on Components and Packaging Technology, Vol 22, No 2, pp 186-190.
101. Liu, J. and Lai, Z. (1999), InterPACK'99, International, InterSociety, Electronic Packaging Technical/Business Conference & Exhibition, June 13-17, Maui, Hawaii, USA, pp. 1691-1697.
102. Helle Westphal, in "Conductive Adhesives for Electronics Packaging," edited by Johan Liu, Electrochemical Publications Ltd, UK, pp. 415-424, 1998.
103. Tomas Segerberg, "Life Cycle Analysis - A comparison between conductive adhesives and lead containing solder for surface mount application, " IVF report,1997.
104. Arne Tolvgård, Jens Malmodin, Johan Liu and Zonghe Lai, Proc. POLY'99.
105. L.Li & J. E. Morris, Int. J. Microelectronic Packaging, 1(3) 1998, 159-175.
106. J. Liu, (editor), Conductive Adhesives for Electronics Packaging, Electrochemical Publications Ltd, 1999, (Port Erin, Isle of Ma n, UK.) ISBN No 0 901 150 37 1.
107. G. Dou, D. C. Whalley, & C. Liu, Proc. 6th IEEE CPMT Confer. High Density Microsystem Design & Packaging & Component Failure Analysis (HDP'04), Shanghai, 2004, pp. 264-276.
108. **J. Liu Dongkai chapter**
109. J. E. Morris and J. Liu, "An Internet Course on Conductive Adhesives for Electronics Packaging," Proc. ECTC'00, Las Vegas, May 2000.
110. J. Liu & J. E. Morris, Proc. Workshop Polymeric Materials for Microelectronics & Photonics Applications, EEP-Vol. 27, ASME, 1999, pp. 259-281.

List of Figures

Figure 1	ICA contact joints: (a) schematic, (b) flip-chip on FR-4, (c) SMT on FR-4.
Figure 2	ACA flip-chip joining: (a) schematic, (b) Ni hard particle filler, (c) metal coated polymer filler, (d) vertical view showing random filler dispersion.
Figure 3	Percolation threshold [2].
Figure 4	ICA bi-modal filler distribution (Ag flakes & powder) with surface layering [4, 6].
Figure 5	Bridging during ACA bonding (Courtesy of Mannan et al) [24].
Figure 6	Probability of particles bridging gap as a function of volume fraction of particles during ACA bonding (Courtesy of Mannan etal) [24].
Figure 7	Resistance dependence on cure as modelled by Equation 7 [4, 6, 27].
Figure 8.	Schematic drawing of the ACA flow during bonding (Courtesy of Mannan et al) [24].
Figure 9	Schematic of metal particles/flakes in an ICA joint, showing sources of resistance [2].
Figure 10	Variation of ICA resistance with track thickness [41].
Figure 11	Log-log resistance variation with thinned thickness. The line of slope for constant bulk resistivity is shown [42].
Figure 12	ICA resistance versus themperature.The slopes match the TCR of Ag [4].
Figure 13	Four-terminal and three-terminal measurements [2, 26]. The test current is injected at the right hand terminal for the usual 4-terminal measurement. Injection into the voltage test terminal includes that contact to the sample. The difference of the two measurements yields the contact resistance.
Figure 14	4-point measurement using ICA track across proto-board current lines [42]. (a) Sense lines short ICA (b) thinned contacts (c) trimmed contacts (d) Surface point contacts
Figure 15	Current crowding effects due to contact track thickness [42]; (a) thin PWB track, (b) thick Cu plates.
Figure 16	ICA drop test improvement from (a) to (b) with pre-heating before cure [77]. Each sample device was dropped 20 times from 1 foot, then 20 times from 2 feet, then 20 times from 3 feet, etc., until failure.
Figure 17.	Schematics of a rigid particle system (Courtesy of Hu et al). [78].
Figure 18.	Schematics of a deformable particle system (Courtesy of Wu et al) [78]..
Figure 19.	Force-resistance-deformation relationship for a deformable particle system (Courtesy of Wu et al) [78].
Figure 20.	Force-resistance-deformation relationship for a rigid particle system (Courtesy of Wu et al) [78].
Figure 21.	The relationship between nickel particle deformation and bonding pressure during ACA flip-chip bonding [80].
Figure 22	(a) Young's Modulus, and (b) Poisson's ratio of ACA film vs. temperature after cure [81].
Figure 23.	Stress profile at the reduction in height of 0.5 μm [20].
Figure 24.	Deformation mechanism of the ACA joint due to thermally induced stress [82]. (a) Strain caused by thermal mismatch cannot change with bump height in ACA joint. (b) Schematic diagram showing that thermal mismatch strain reduces as bump height increases for solder joints.
Figure 25	ICA resistance and surface temperature, as current is increased to thermal runaway and destruction [41]. The straight line corresponds to internal temperatures estimated from the resistance and the TCR.
Figure 26	Series contact resistance of 10 epoxy-based ICA mounted chip components in series, before and after 1000 hours of 85°C and 85% RH [89]. (a) Sn37Pb plated chips and boards; (b) Ag/Pd plated chips and Au plated boards
Figure 27	Average shear strength of 10 epoxy-based ICA-mounted chip components in series, before and after 1000 hours of 85°C and 85% RH [90]. (a) Sn37Pb plated chips and boards; (b) Ag/Pd plated chips and Au plated boards.
Figure 28	FTIR results for cured ACAs [92]. (i) FTIR Spectra (a) after 41 hours of 85/85 testing, (b) before the testing, and (c) the difference spectrum. (ii) Difference spectra for (a) 41 hours, (b) 162 hours, and (c) 821 hours at 85/85.

Figurre 29 Post-cure resistance changes for an Ag-filled ICA [4, 6, 27]. (a) Bulk resistance; (b) contact resistance to Au; (c) contact resistance to Cu.
Figure 30 Strain cycling joint lifetimes according to the Coffin-Manson equation [97].
Figure 31 High temperature cycling [98]. (a) Type 2 joint failures occur at higher temperatures; (b) Type 3 joint failures occur at lower temperatures; (c) Type 4 joint failure occur in both high & low temperature regions.
Figure 32. Schematics of four types of ACA joints caused by different bump geometries, variations in filler size, and differences in bonding pressure [98]. The classifications correspond to Figure 31.
Figure 33. The case on the left is located close the glass fibres (a) and has an excellent resistance (5 mΩ) and reliability, whereas the latter (b) has a high contact resistance (14 mΩ) and poor reliability (49 mΩ after 1000 cycles of TC test) due to its location far from the fibres [100].
Figure 34. Pad sinking led to the bad bonding quality [100].
Figure 35. Cumulative failure of an epoxy based ACA joint in after a temperature cycling test from -40 to +125°C with a dwell time of 15 min at hold temperatures [101].
Figure 36. Electrical resistance of a daisy chain versus the number of cycles of low-cycle fatigue testing. (a) Dry environment; (b) 85°C and 85%RH [81].

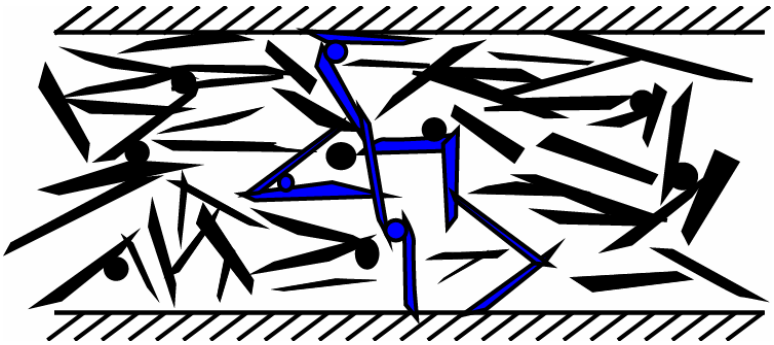

(a)

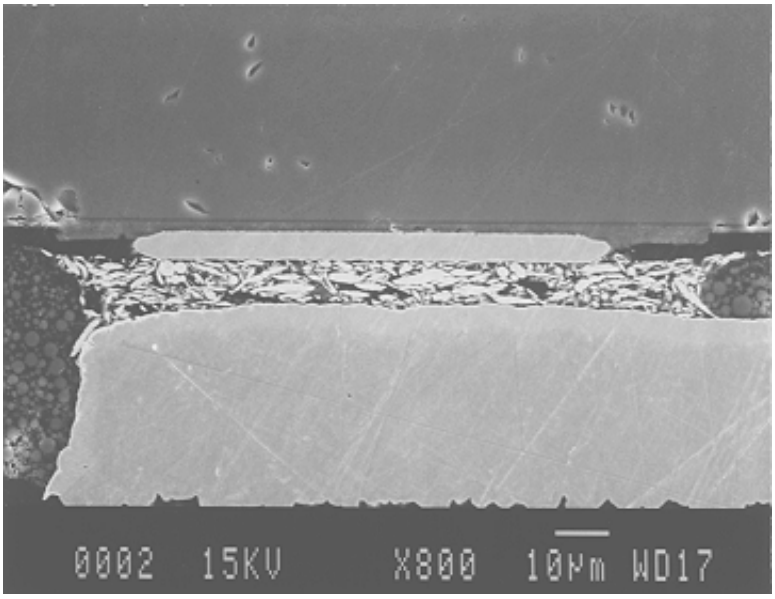

(b)

(c)

Figure 1 ICA contact joints: (a) schematic, (b) flip-chip on FR-4, (c) SMT on FR-4.

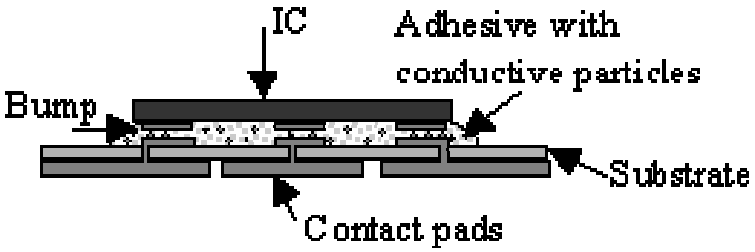

(a)

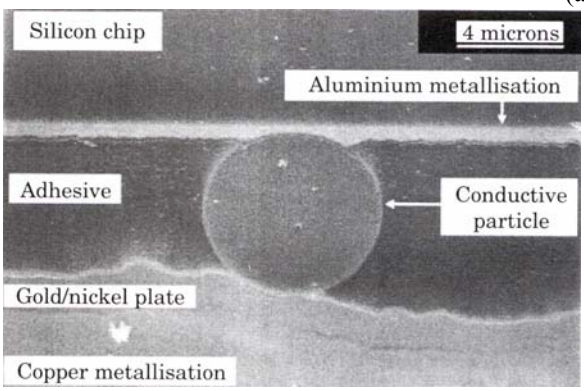

(b)

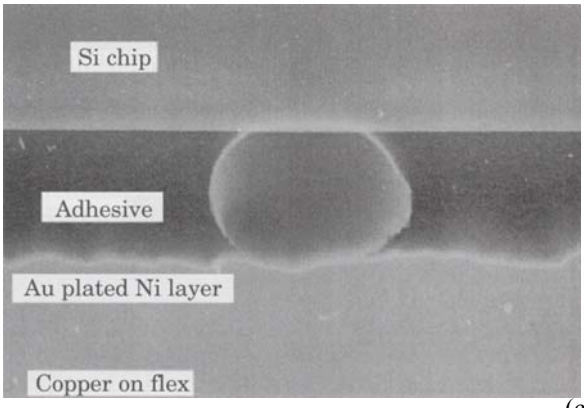

(c)

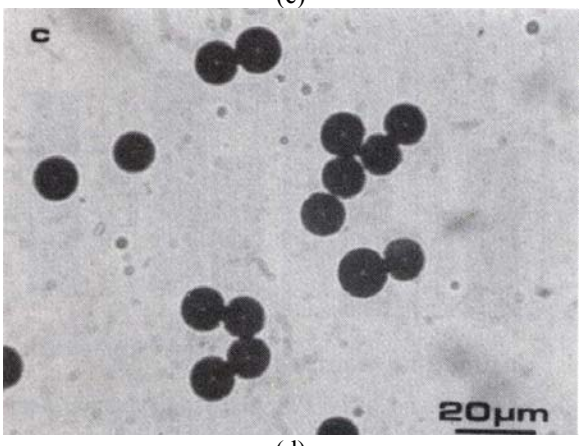

(d)

Figure 2 ACA flip-chip joining: (a) schematic, (b) Ni hard particle filler, (c) metal coated polymer filler, (d) vertical view showing random filler dispersion.

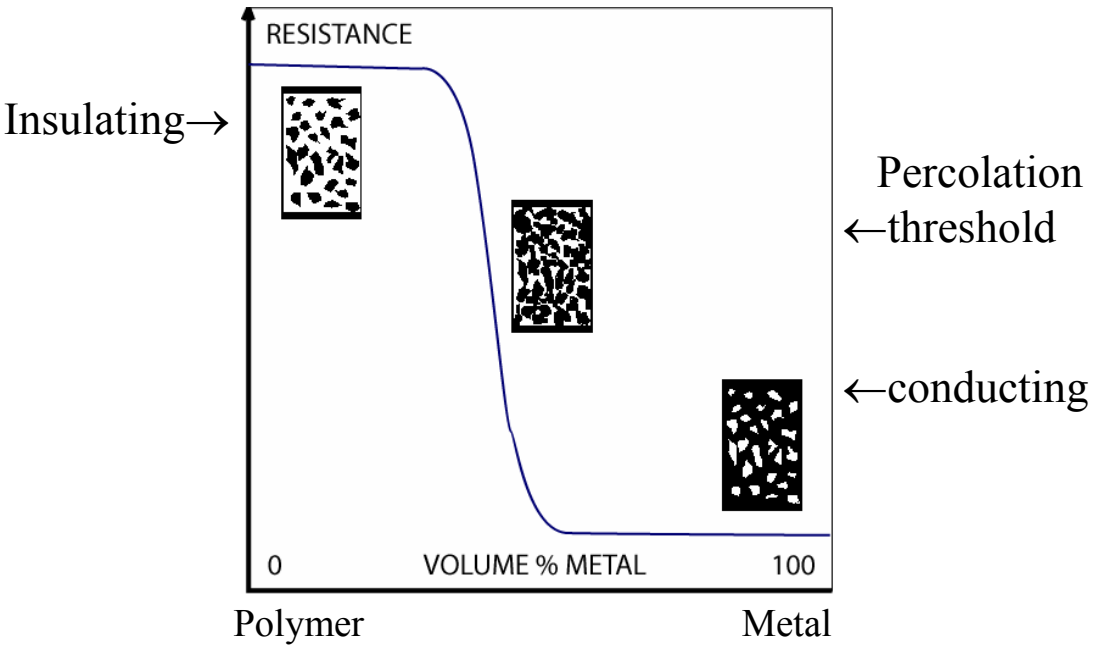

Figure 3 Percolation threshold

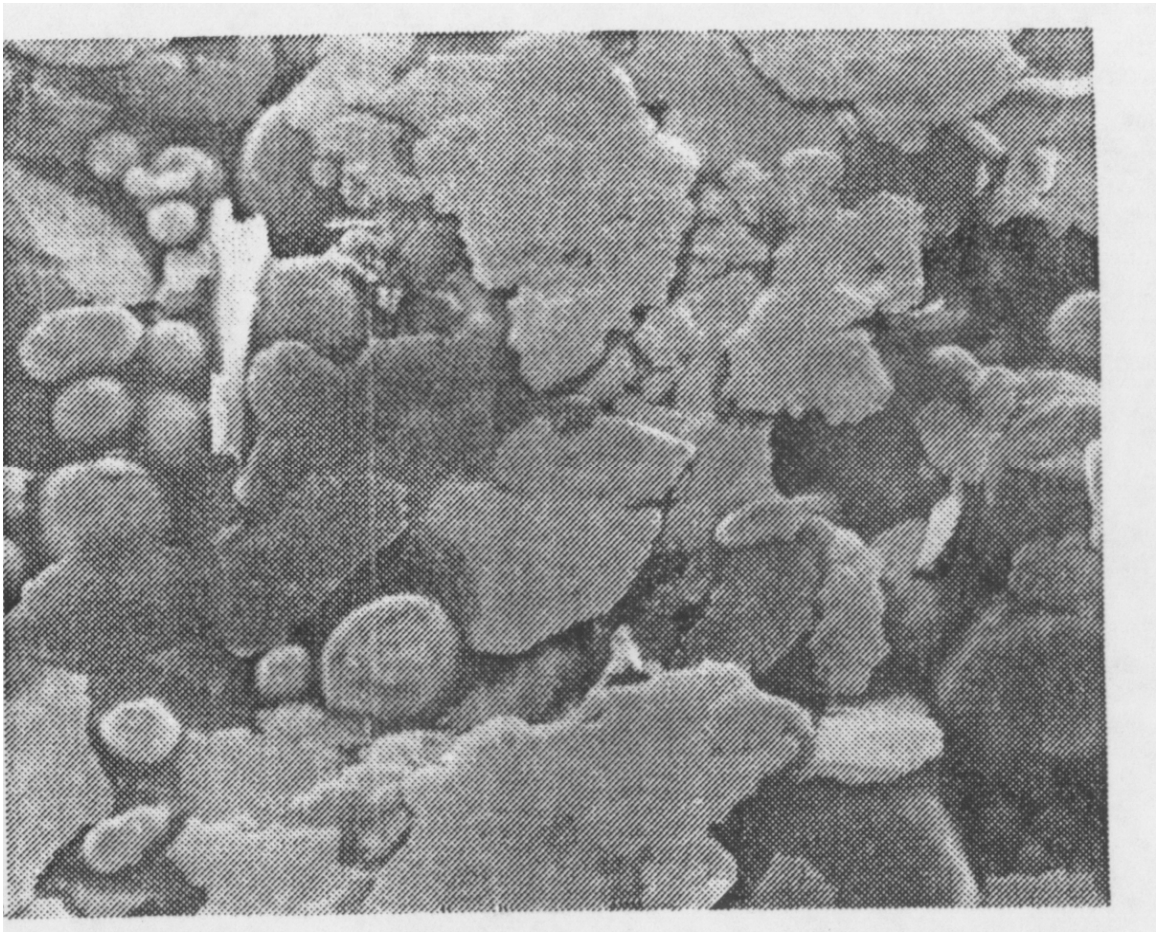

Figure 4 ICA bi-modal filler distribution (Ag flakes & powder) with surface layering.

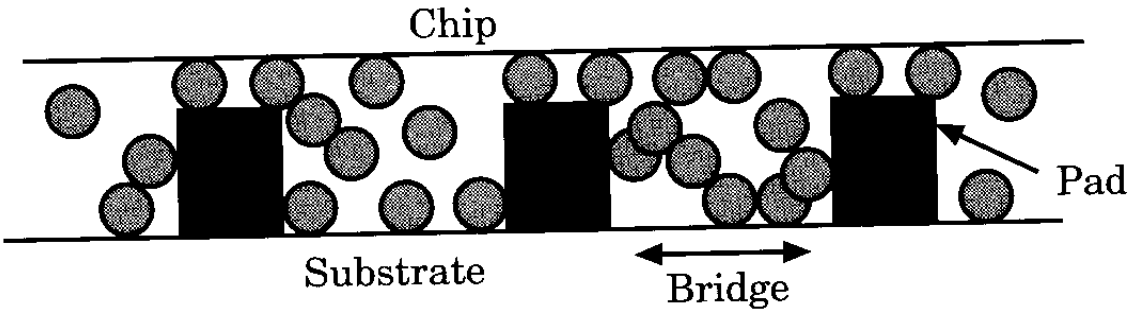

Figure 5 Bridging during ACA bonding (Courtesy of Mannan).

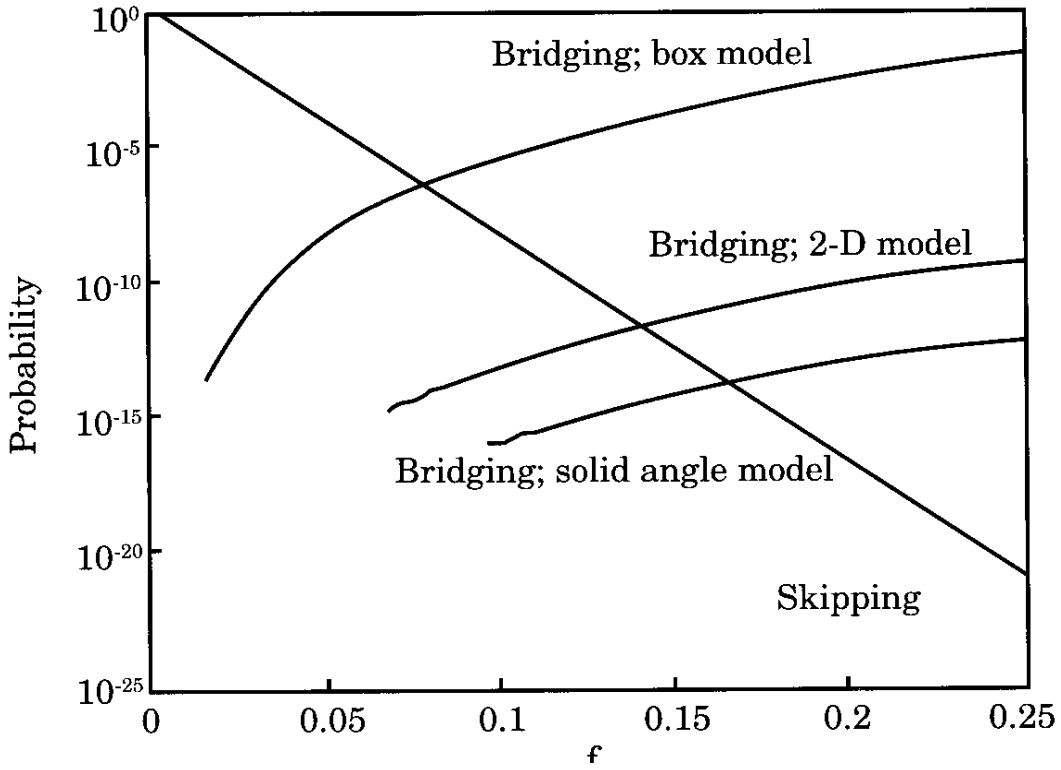

Figure 6 Probability of particles bridging gap as a function of volume fraction of particles during ACA bonding (Courtesy of Mannan, Whalley and Williams).

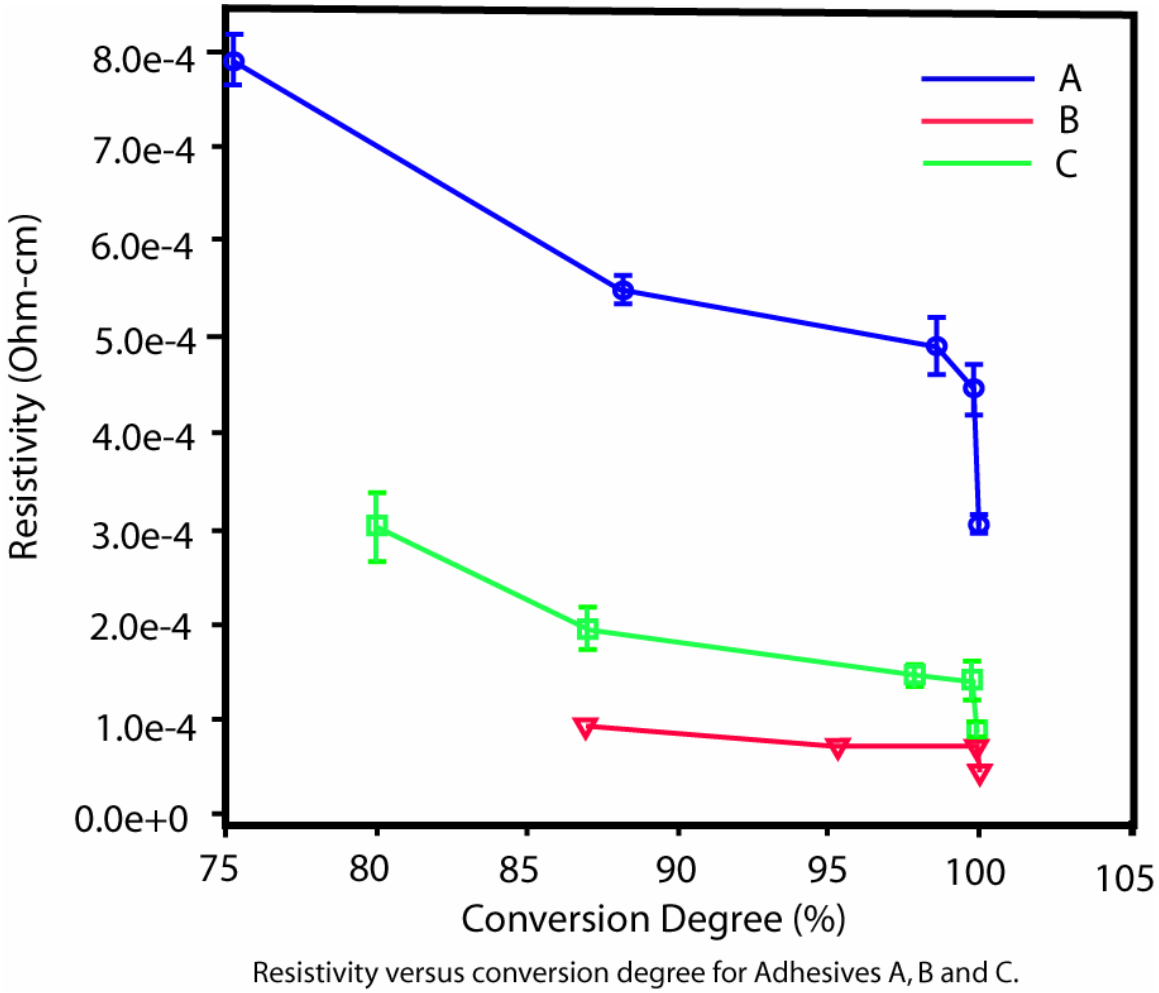

Figure 7 Resistance dependence on cure as modelled by Equation 7.

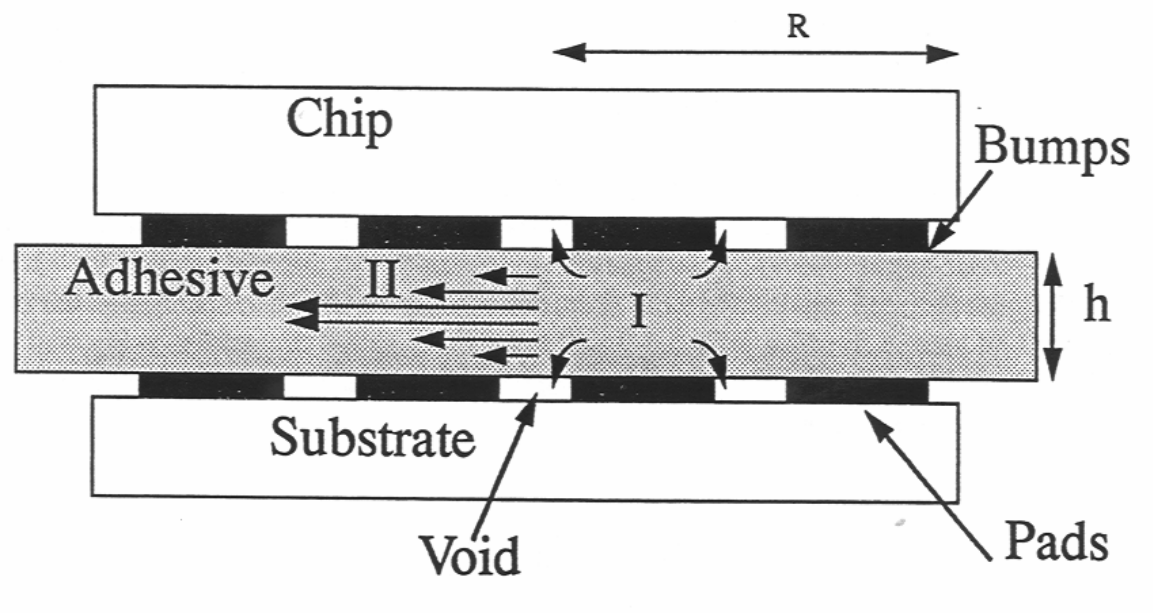

Figure 8. Schematic drawing of the ACA flow during the bonding (Courtesy of Mannan et al).

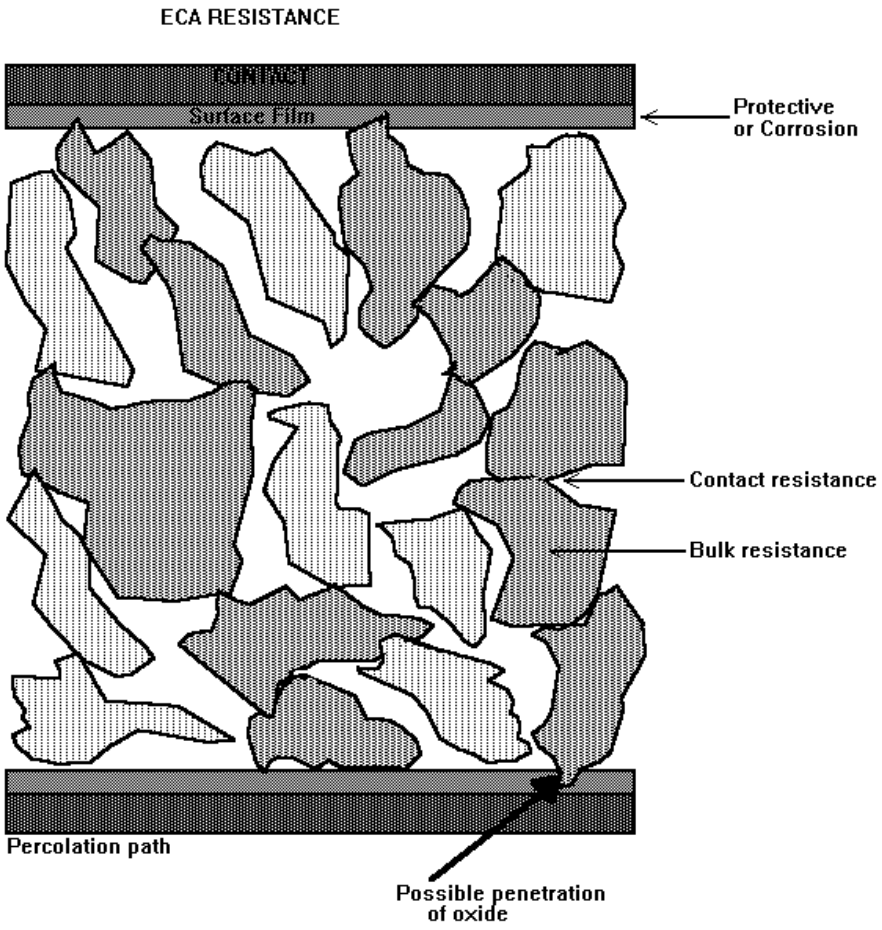

Figure 9 Schematic of metal particles/flakes in an ICA joint, showing sources of resistance.

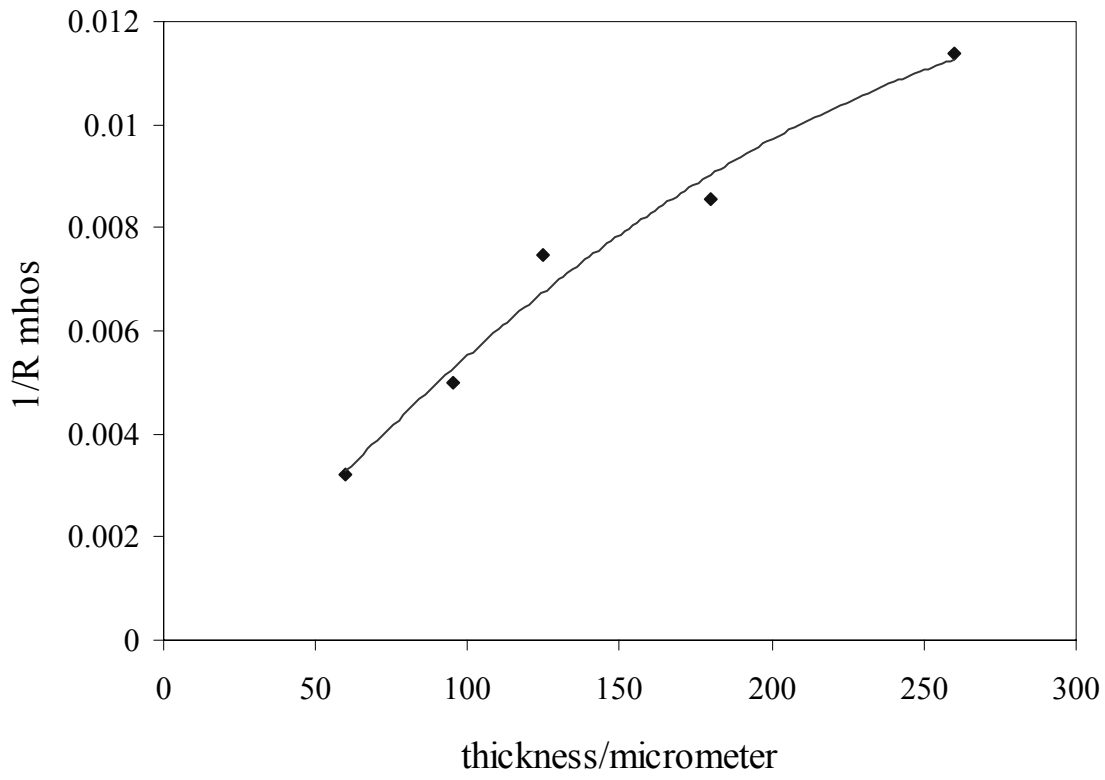

Figure 10 Variation of ICA resistance with track thickness

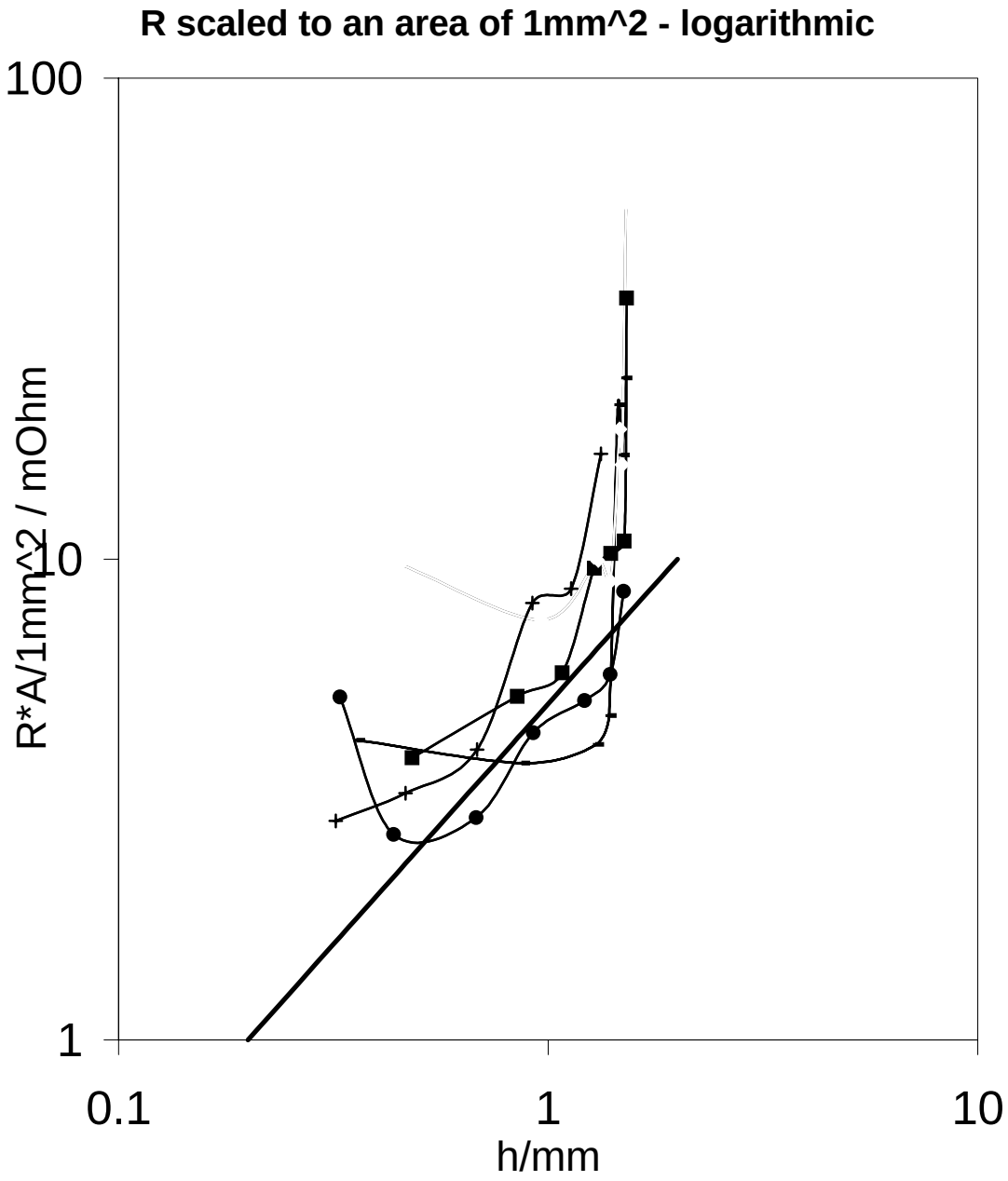

Figure 11 Log-log resistance variation with thinned thickness. The line of slope for constant bulk resistivity is shown.

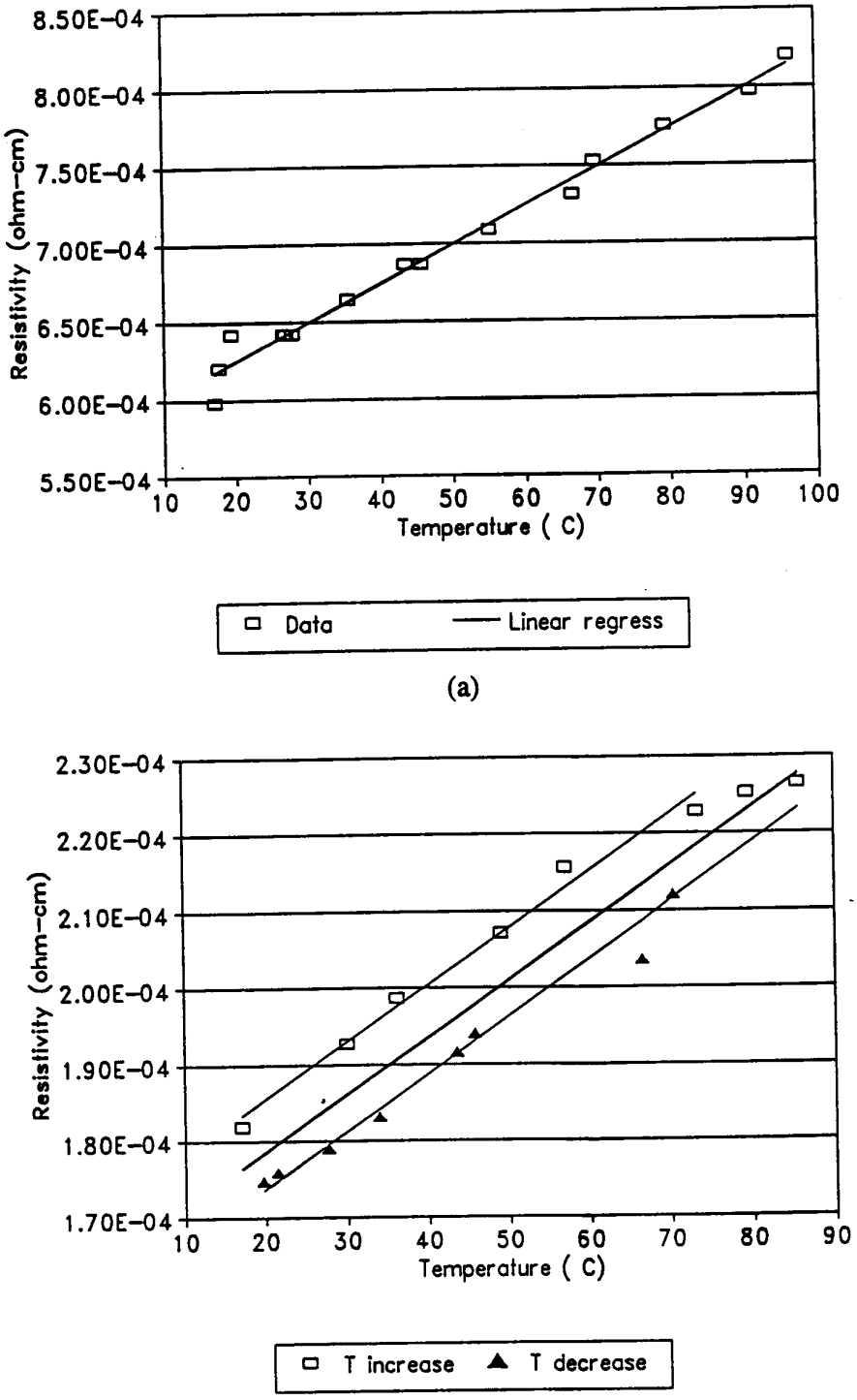

Figure 3.1: Resistivities for various temperatures. (a) Brass stenciled CT-5047-02 thermoset sample (TCR= 0.0039/°C). (b) CSM-933-65-1 screen printed thermoplastic sample. (TCR= 0.0038/°C)

Figure 12 [4]. ICA resistance versus themperature.The slopes match the TCR of Ag.

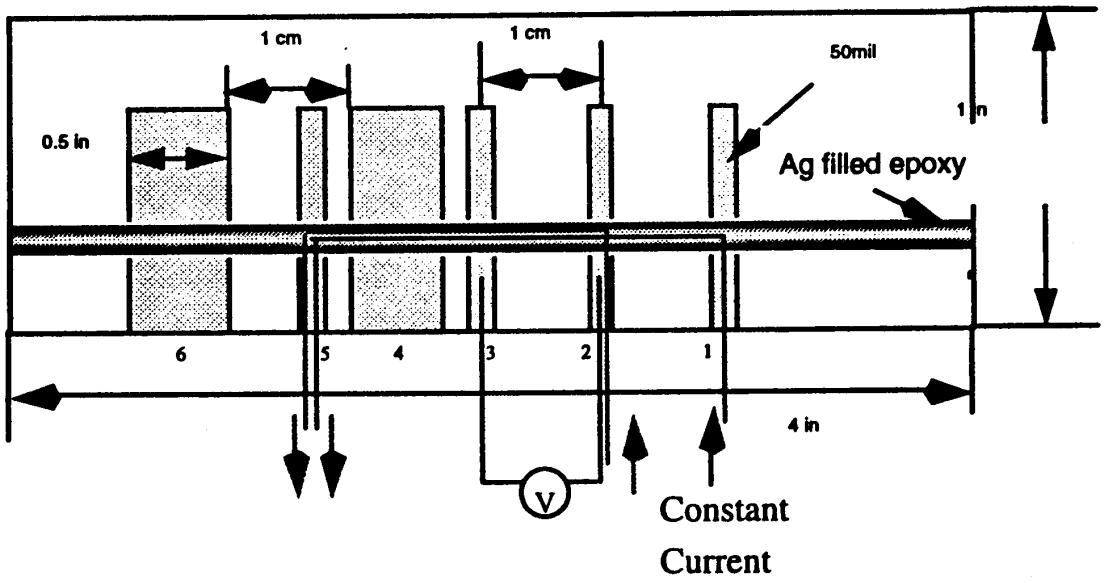

Figure 13 Four-terminal and three-terminal measurements. The test current is injected at the right hand terminal for the usual 4-terminal measurement. Injection into the voltage test terminal includes that contact to the sample. The difference of the two measurements yields the contact resistance.

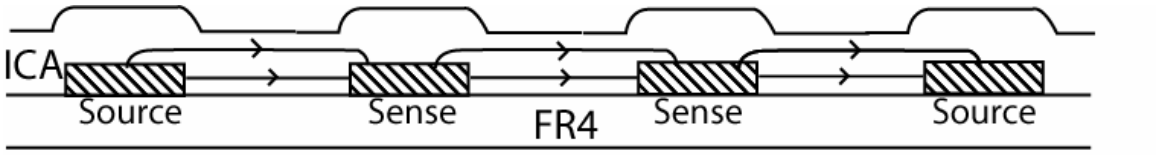

(a)

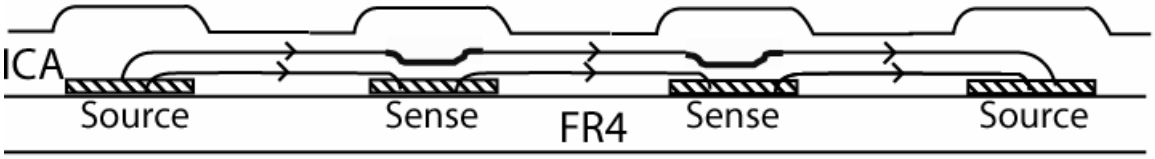

(b)

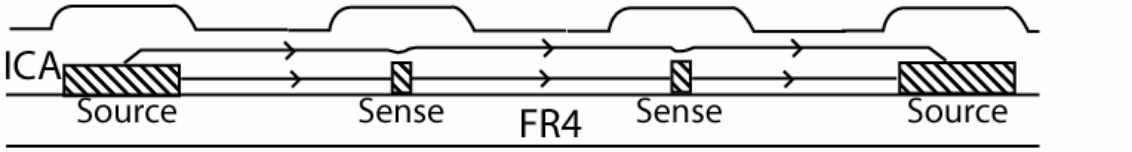

(c)

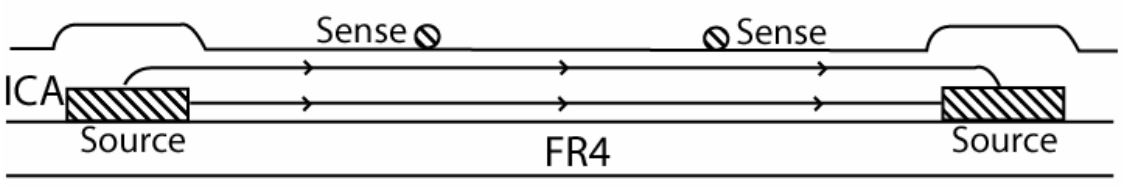

(d)

Figure 14 4-point measurement using ICA track across proto-board current lines (a) Sense lines short ICA (b) thinned contacts (c) trimmed contacts (d) Surface point contacts

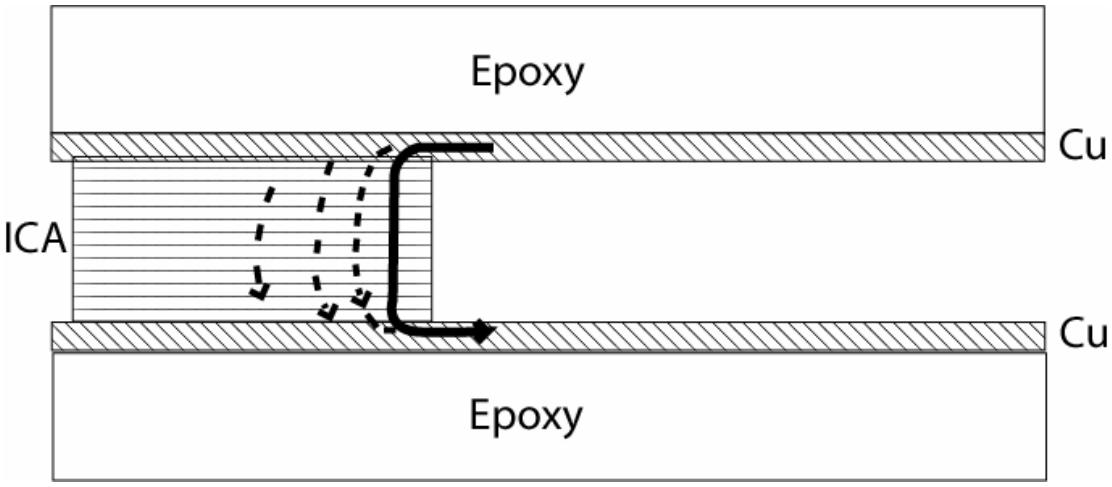

(a)

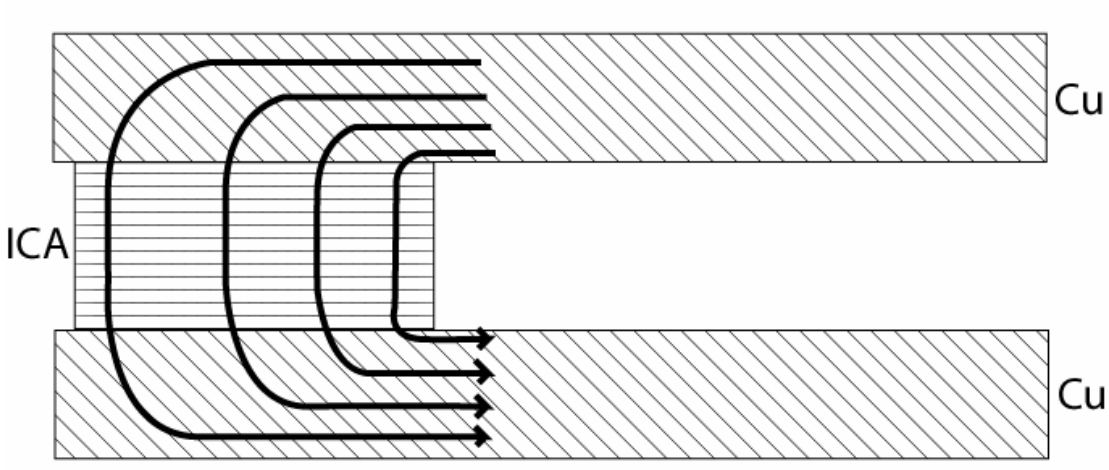

(b)

Figure 15 Current crowding effects due to contact track thickness; (a) thin PWB track, (b) thick Cu plates.

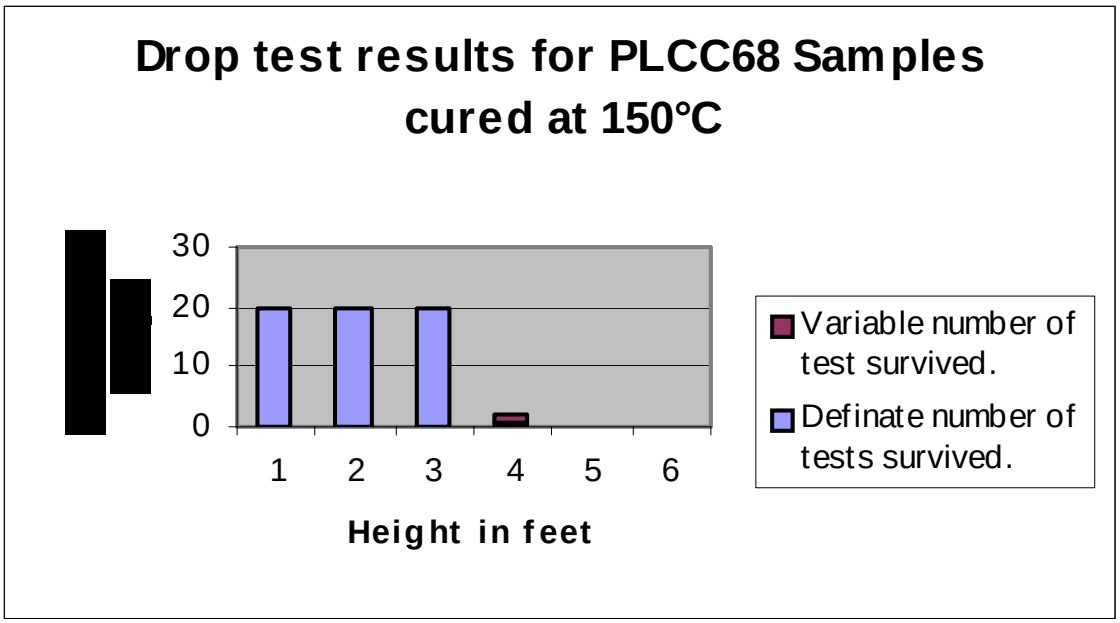

(a)

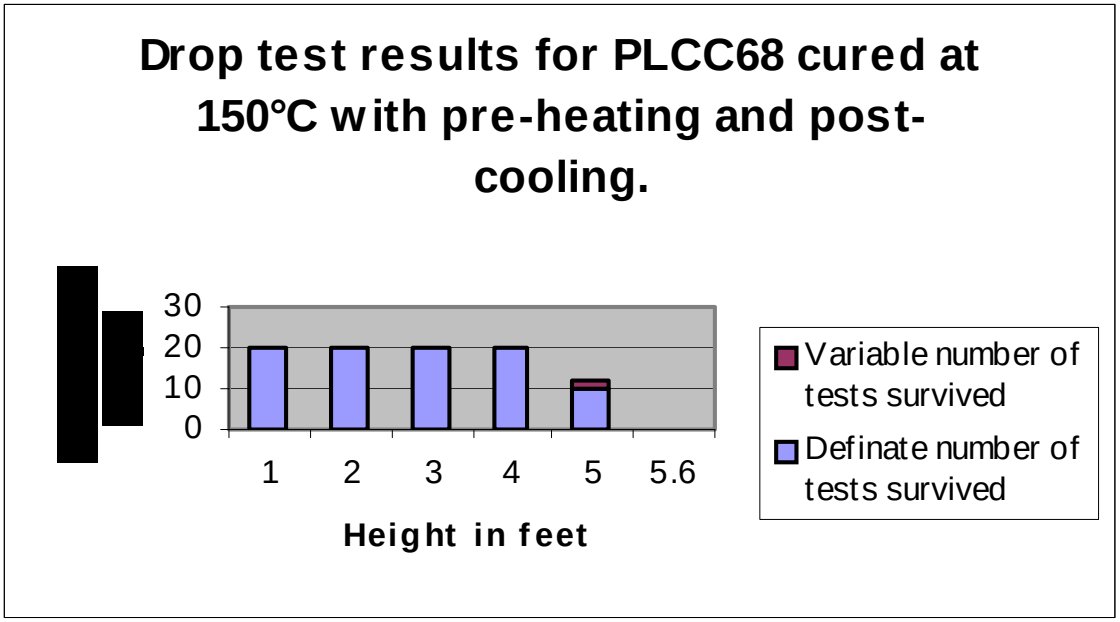

(b)

Figure 16 ICA drop test improvement from (a) to (b) with pre-heating before cure. Each sample device was dropped 20 times from 1 foot, then 20 times from 2 feet, then 20 times from 3 feet, etc., until failure.

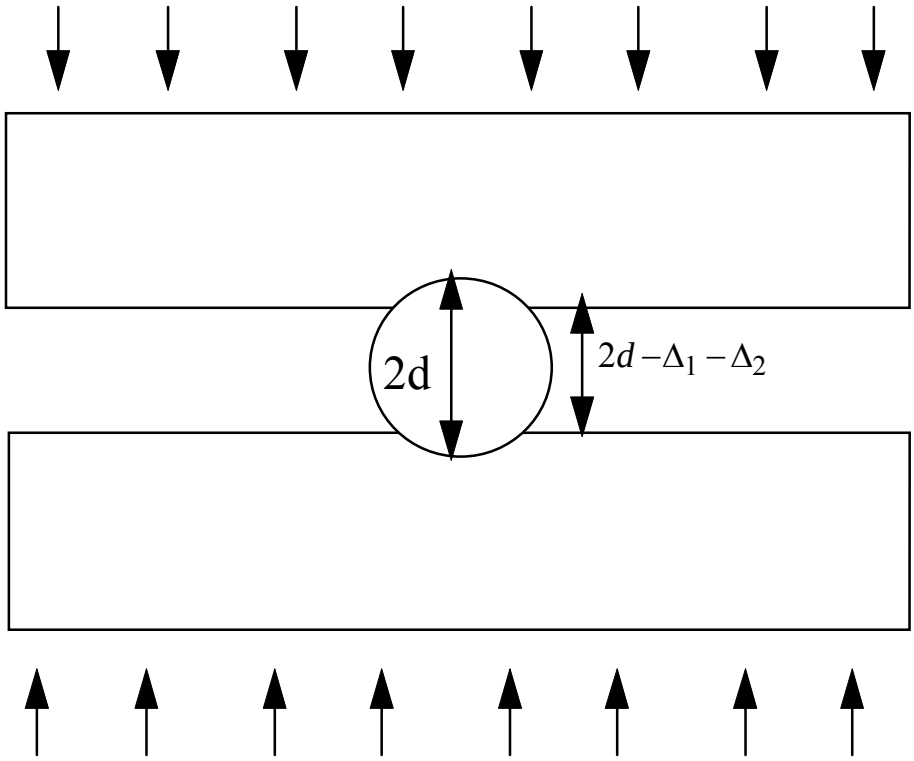

Figure 17. Schematics of a rigid particle system (Courtesy of Hu et al).

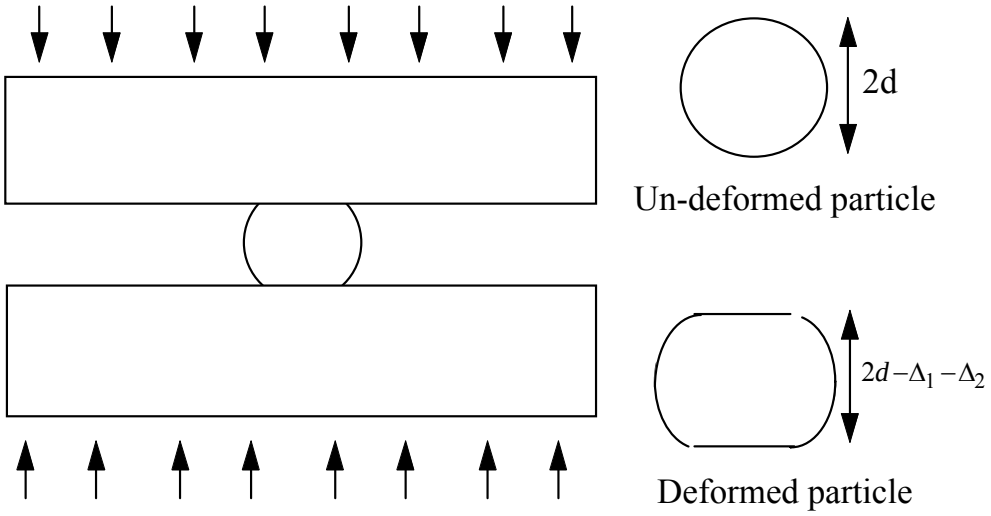

Figure 18. Schematics of a deformable particle system (Courtesy of Wu et al).

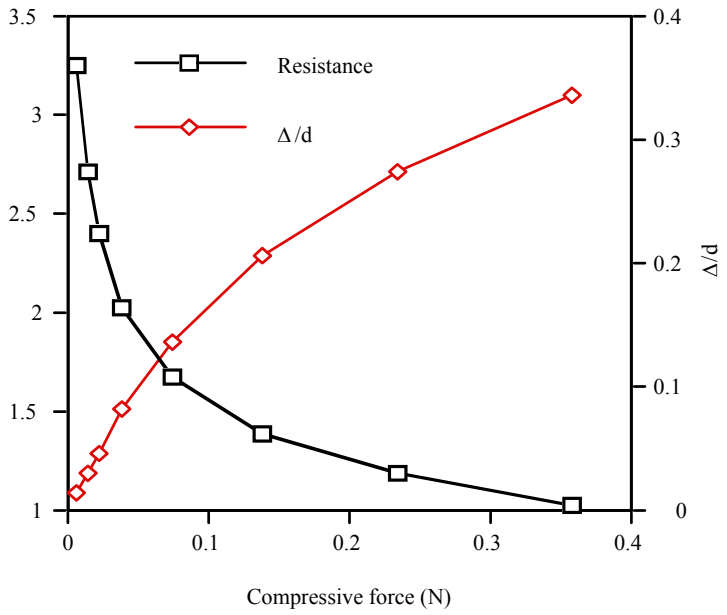

Figure 19. Force-resistance-deformation relationship for a deformable particle system (Courtesy of Wu et al).

.

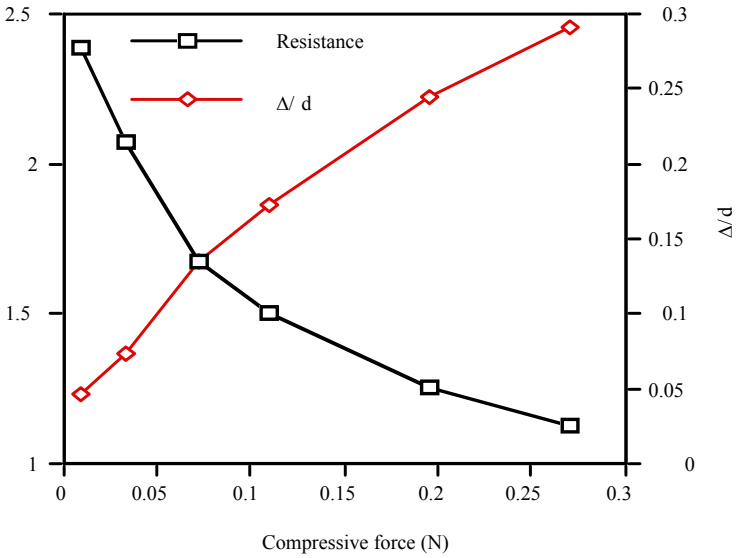

Figure 20. Force-resistance-deformation relationship for a rigid particle system (Courtesy of Wu et al).

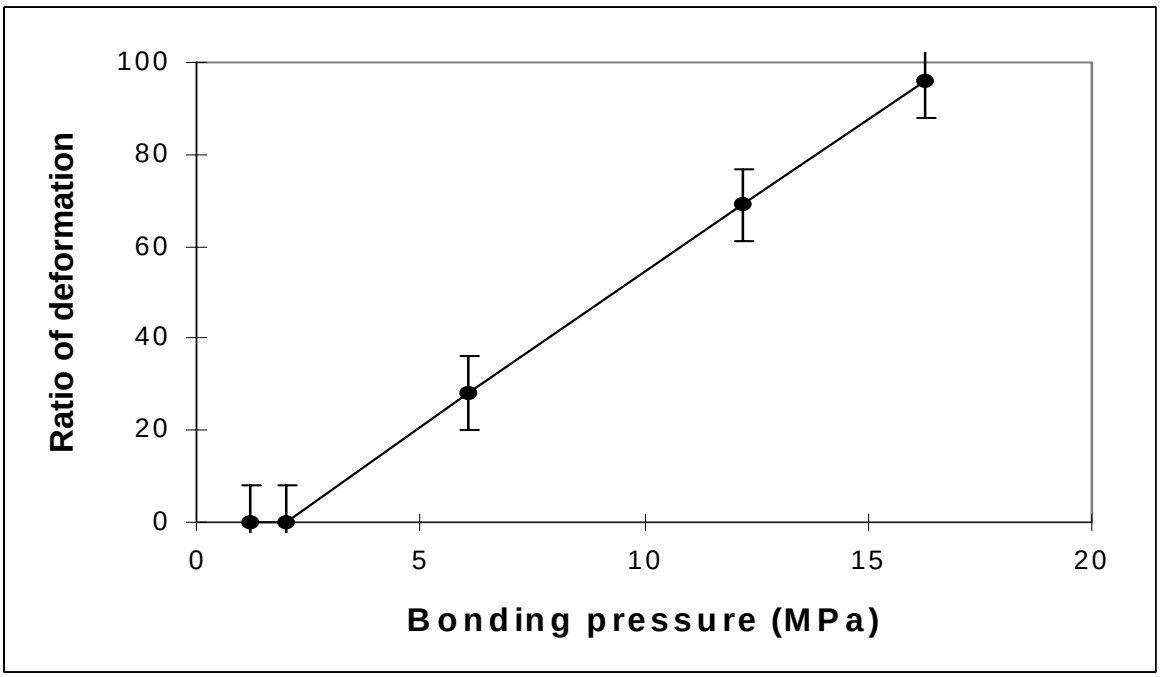

Figure 21. The relationship between nickel particle deformation and bonding pressure during ACA flip-chip bonding.

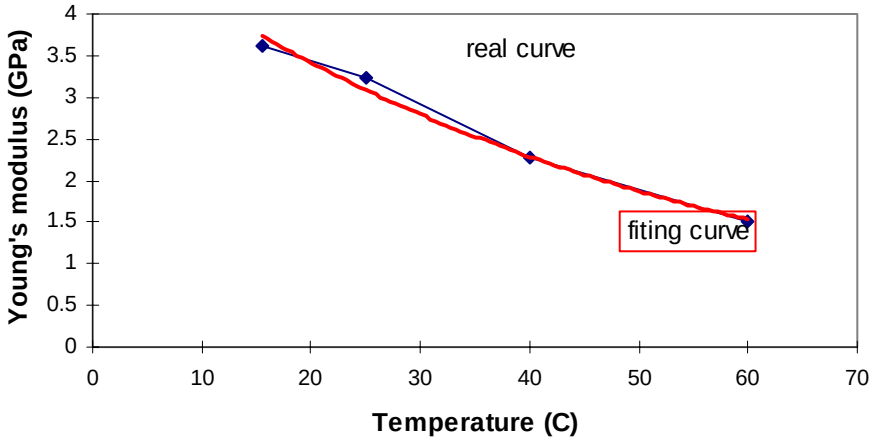

(a)

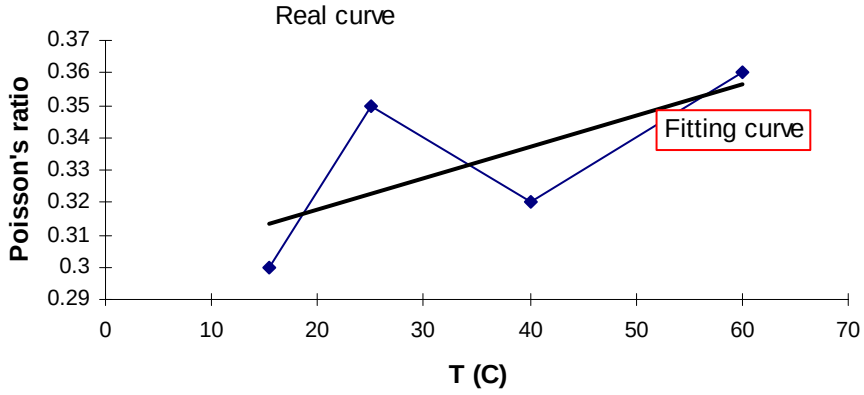

(b)

Figure 22 (a) Young's Modulus, and (b) Poisson's ratio of ACA film vs. temperature after cure.

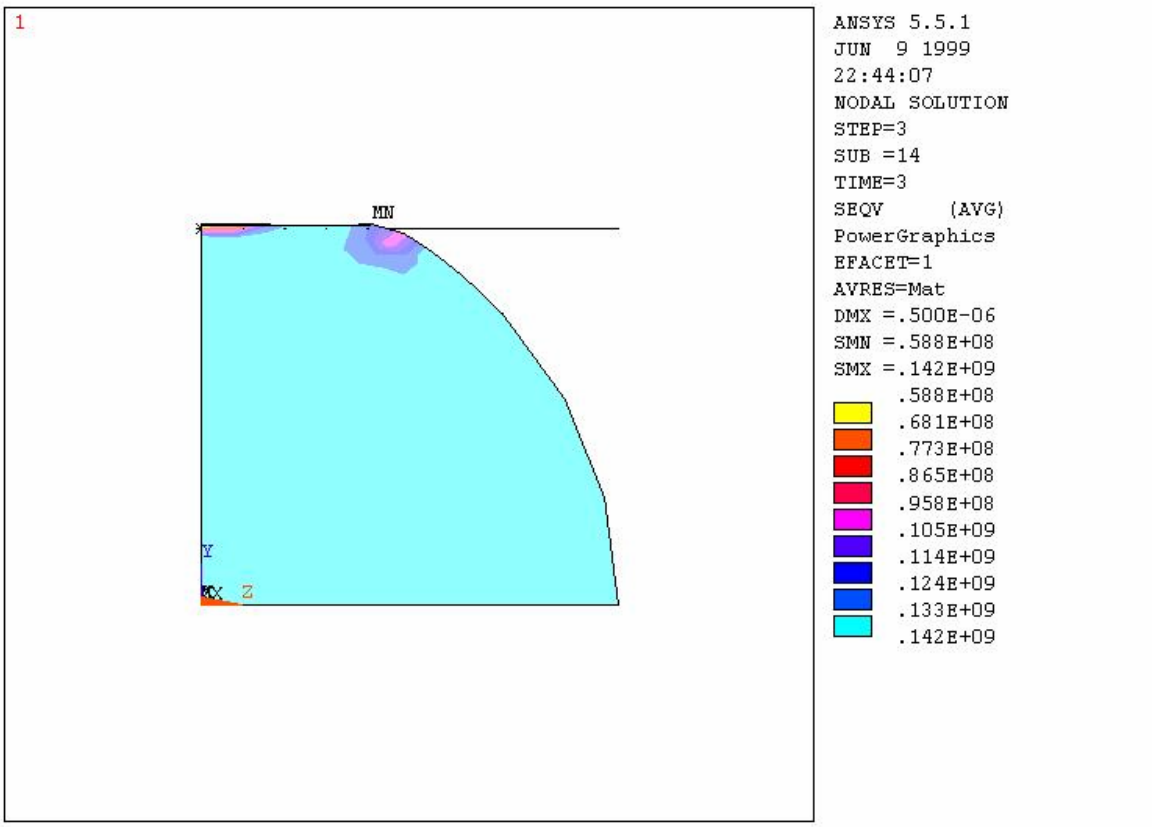

Figure 23. Stress profile at the reduction in height of 0.5 □m [20].

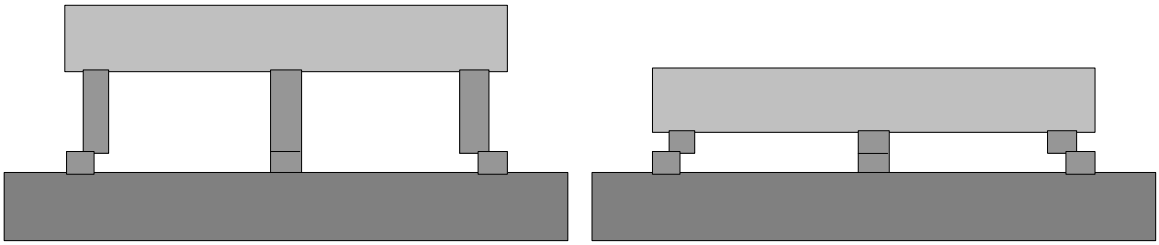

(a)

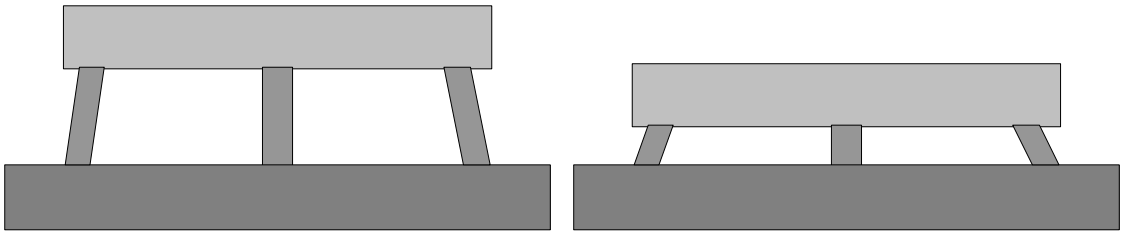

(b)

Figure 24. Deformation mechanism of the ACA joint due to thermally induced stress. (a) Strain caused by thermal mismatch cannot change with bump height in ACA joint. (b) Schematic diagram showing that thermal mismatch strain reduces as bump height increases for solder joints.

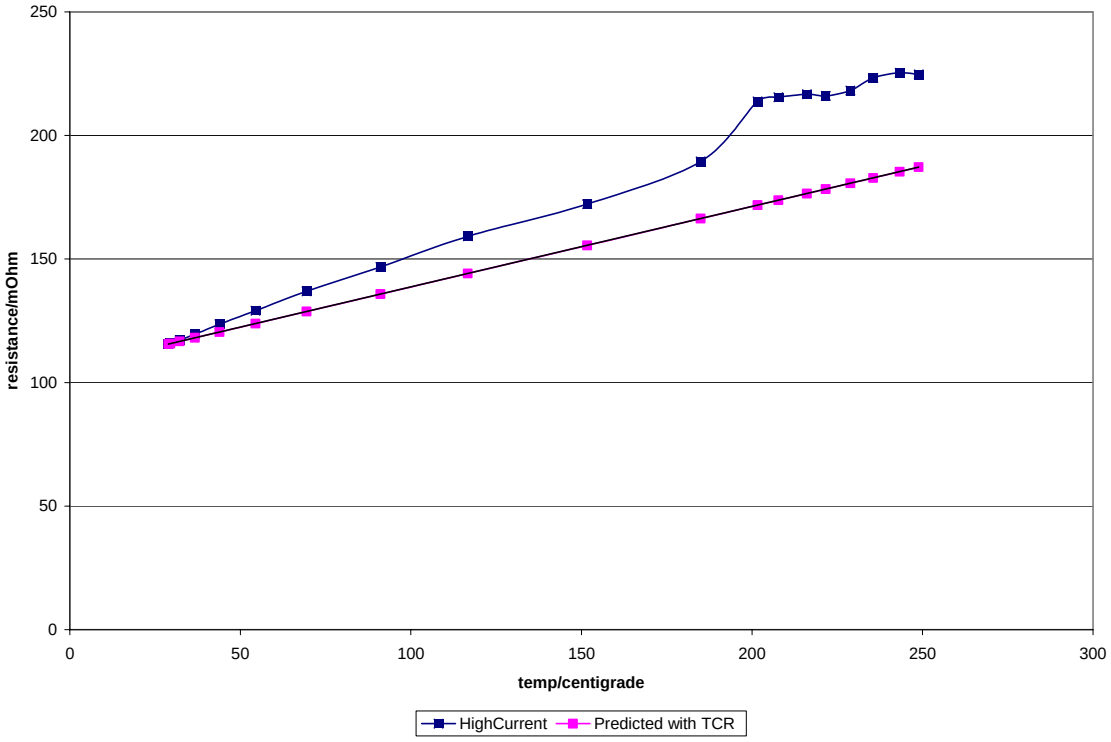

Figure 25 ICA resistance and surface temperature, as current is increased to thermal runaway and destruction. The straight line corresponds to internal temperatures estimated from the resistance and the TCR.

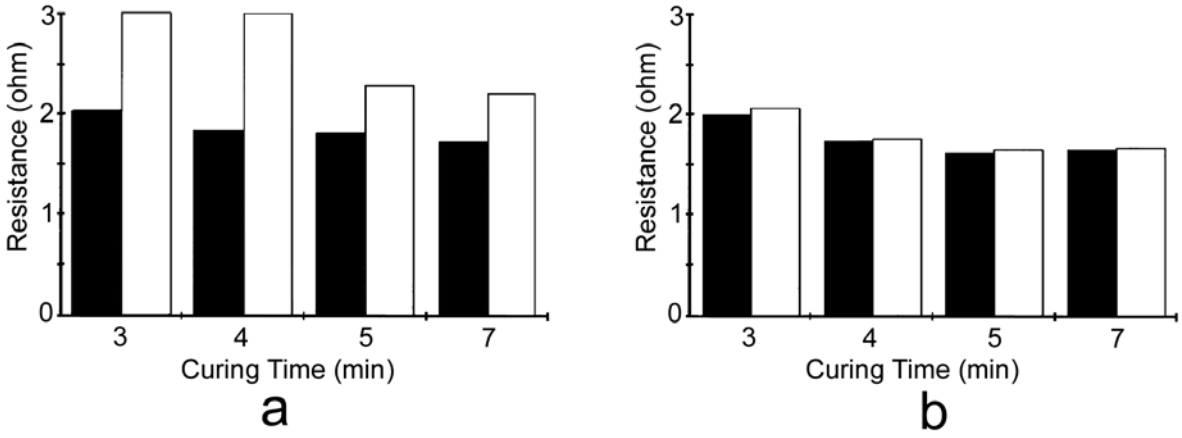

Figure 26 Series contact resistance of 10 epoxy-based ICA mounted chip components in series, before and after 1000 hours of 85°C and 85% RH. (a) Sn37Pb plated chips and boards; (b) Ag/Pd plated chips and Au plated boards.

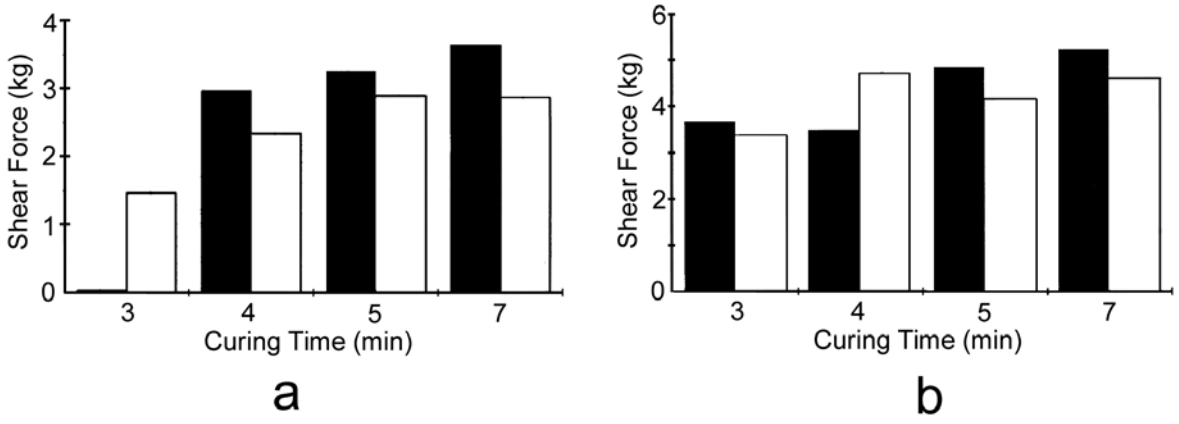

Figure 27 Average shear strength of 10 epoxy-based ICA mounted chip components in series, before and after 1000 hours of 85°C and 85% RH. (a) Sn37Pb plated chips and boards; (b) Ag/Pd plated chips and Au plated boards.

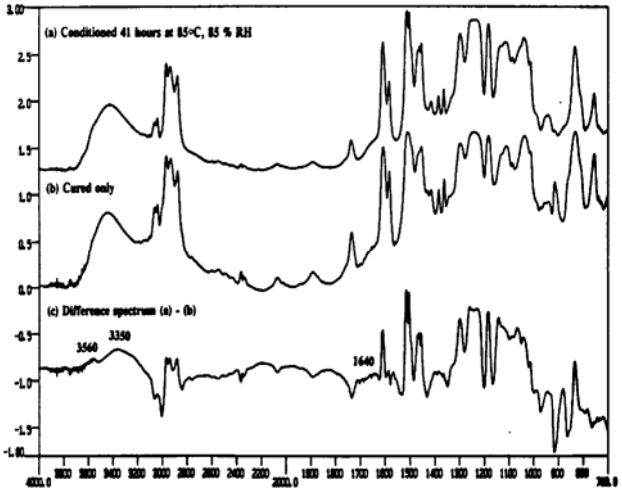

(i)

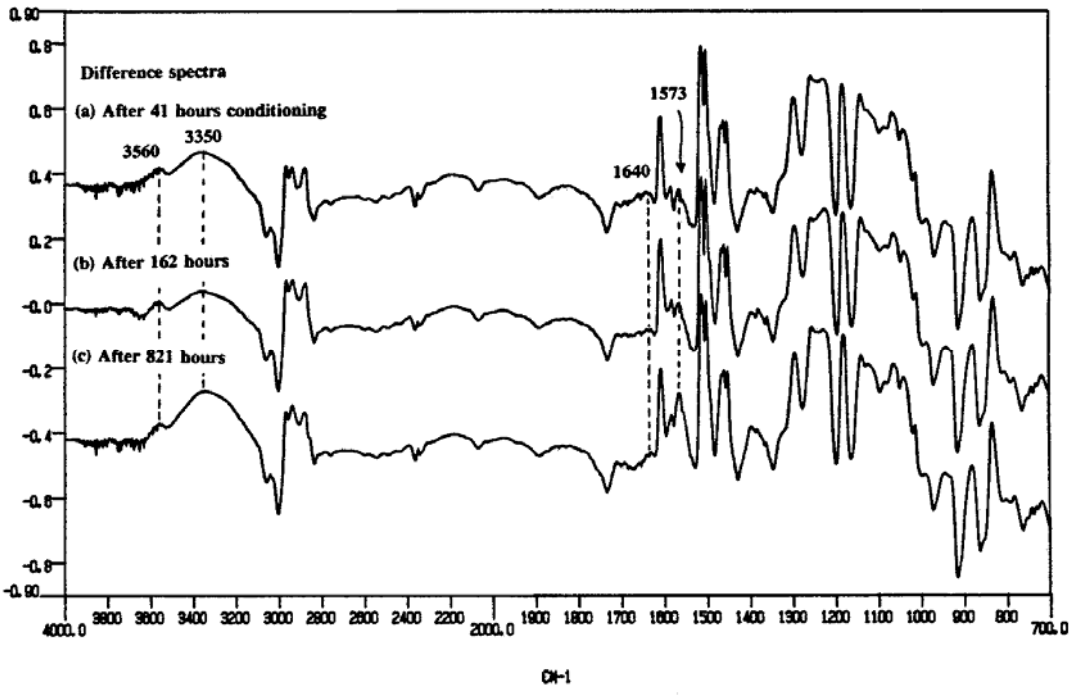

(ii)

Figure 28 FTIR results for cured ACAs. (i) FTIR Spectra (a) after 41 hours of 85/85 testing, (b) before the testing, and (c) the difference spectrum. (ii) Difference spectra for (a) 41 hours, (b) 162 hours, and (c) 821 hours at 85/85.

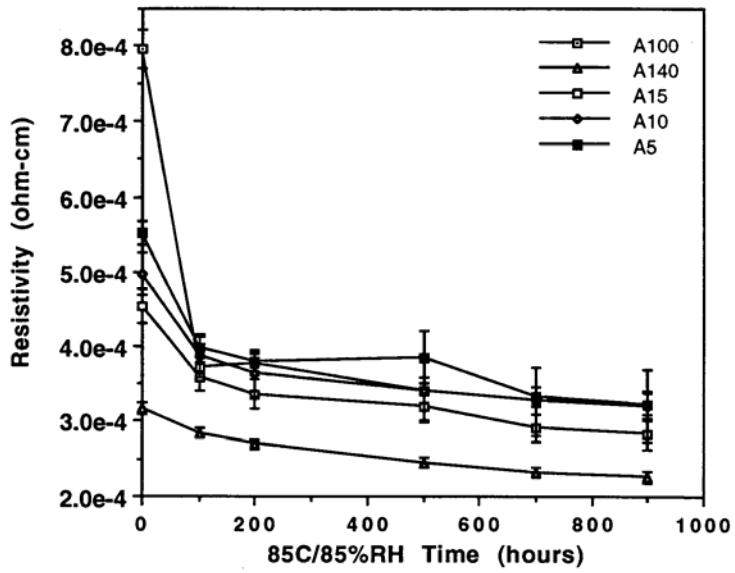

(a)

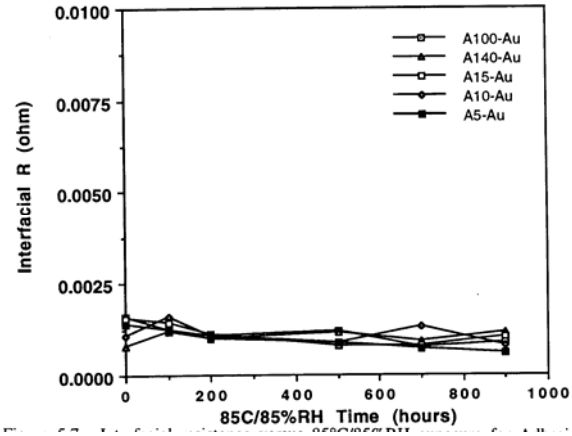

(b)

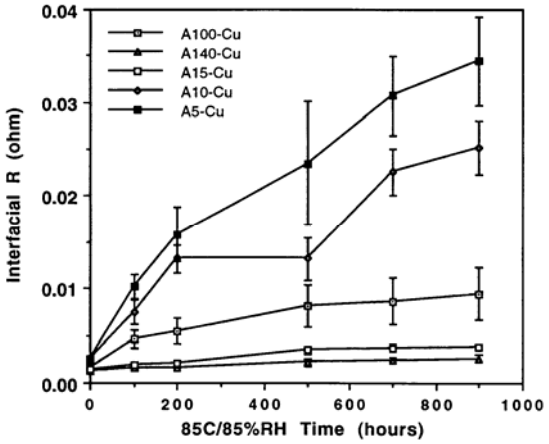

(c)

Figurre 29 Post-cure resistance changes for an Ag-filled ICA. (a) Bulk resistance; (b) contact resistance to Au; (c) contact resistance to Cu.

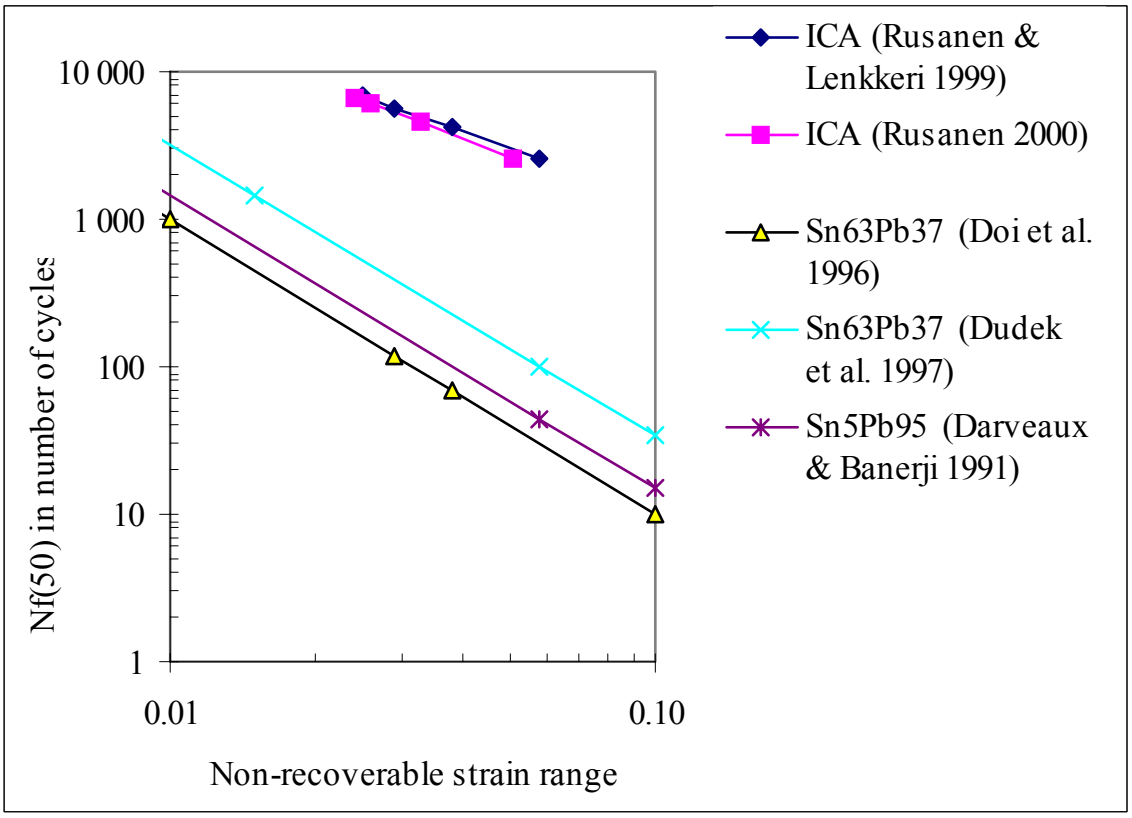

Figure 30 Strain cycling joint lifetimes according to the Coffin-Manson equation

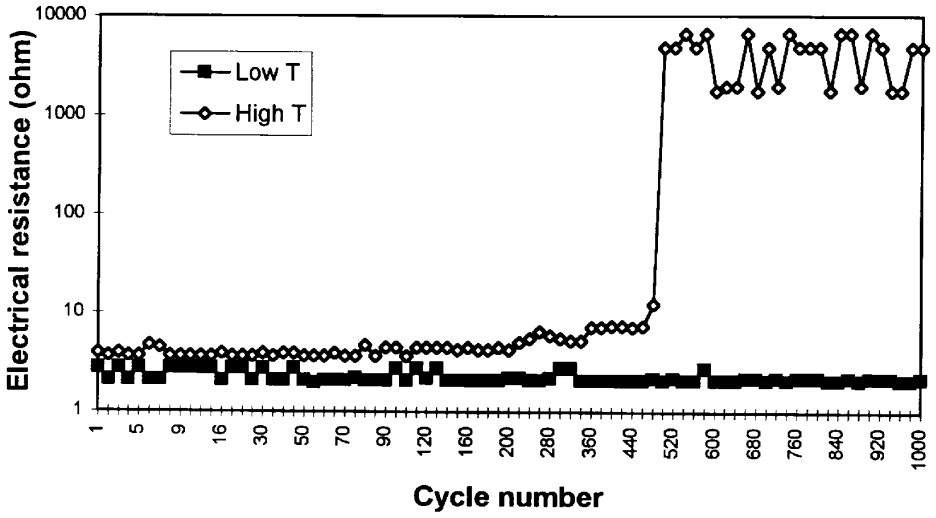

(a).

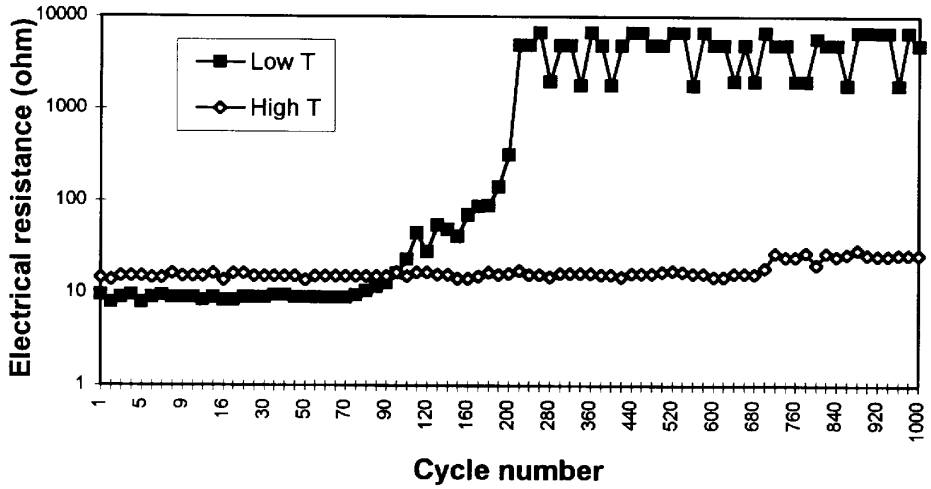

(b)

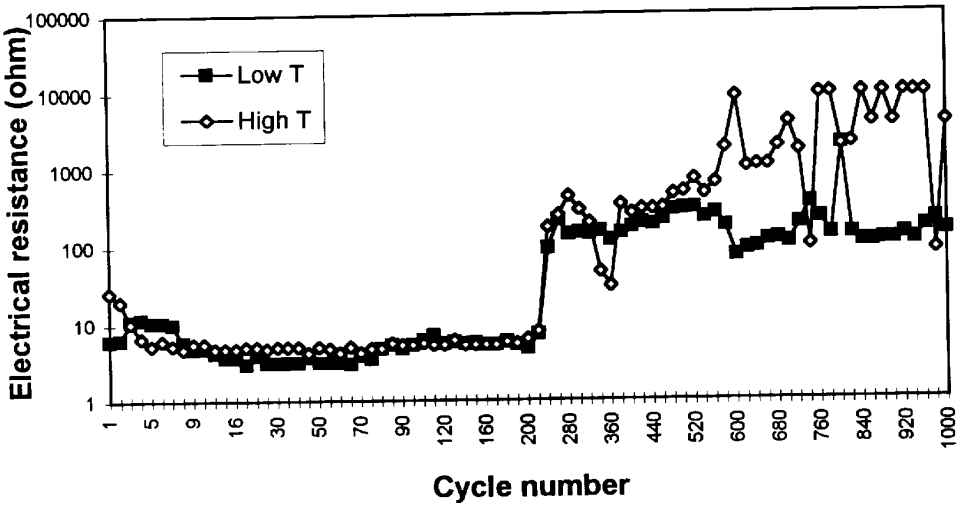

(c)

Figure 31 High temperature cycling. (a) Type 2 joint failures occur at higher temperatures; (b) Type 3 joint failures occur at lower temperatures; (c) Type 4 joint failure occur in both high & low temperature regions.

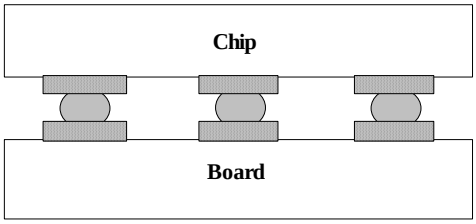

Type 1, the most reliable structure.

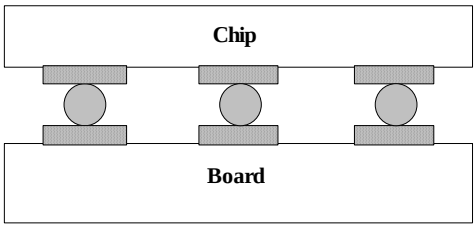

Type 2, unstable at high temperature.

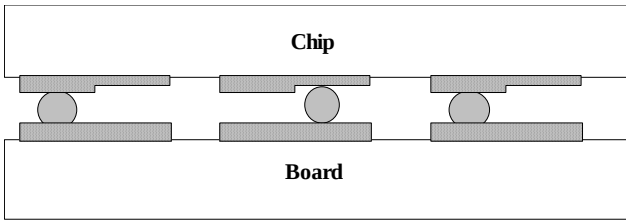

Type 3, unstable at low temperature.

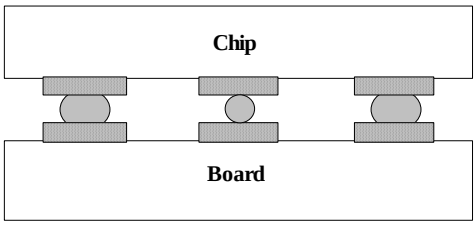

Type 4, unstable when temperature changes.

Figure 32. Schematics of four types of ACA joints caused by different bump geometries, variations in filler size, and differences in bonding pressure. The classifications correspond to Figure 31.

Figure 33. The case in the left is located close the glass fibres (a) and has an excellent resistance (5 mΩ) and reliability, whereas the latter (b) has a high contact resistance (14 mΩ) and poor reliability (49 mΩ after 1000 cycles of TC test) due to its location far from the fibres.

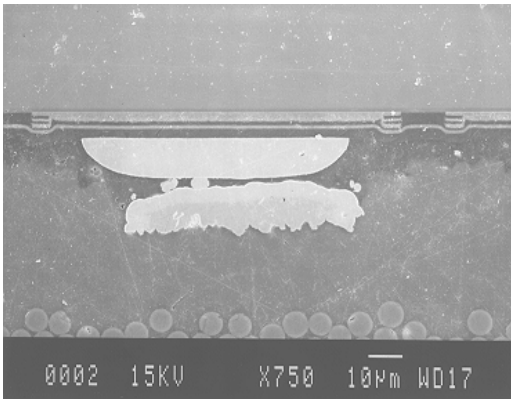

Figure 34. Pad sinking led to the bad bonding quality.

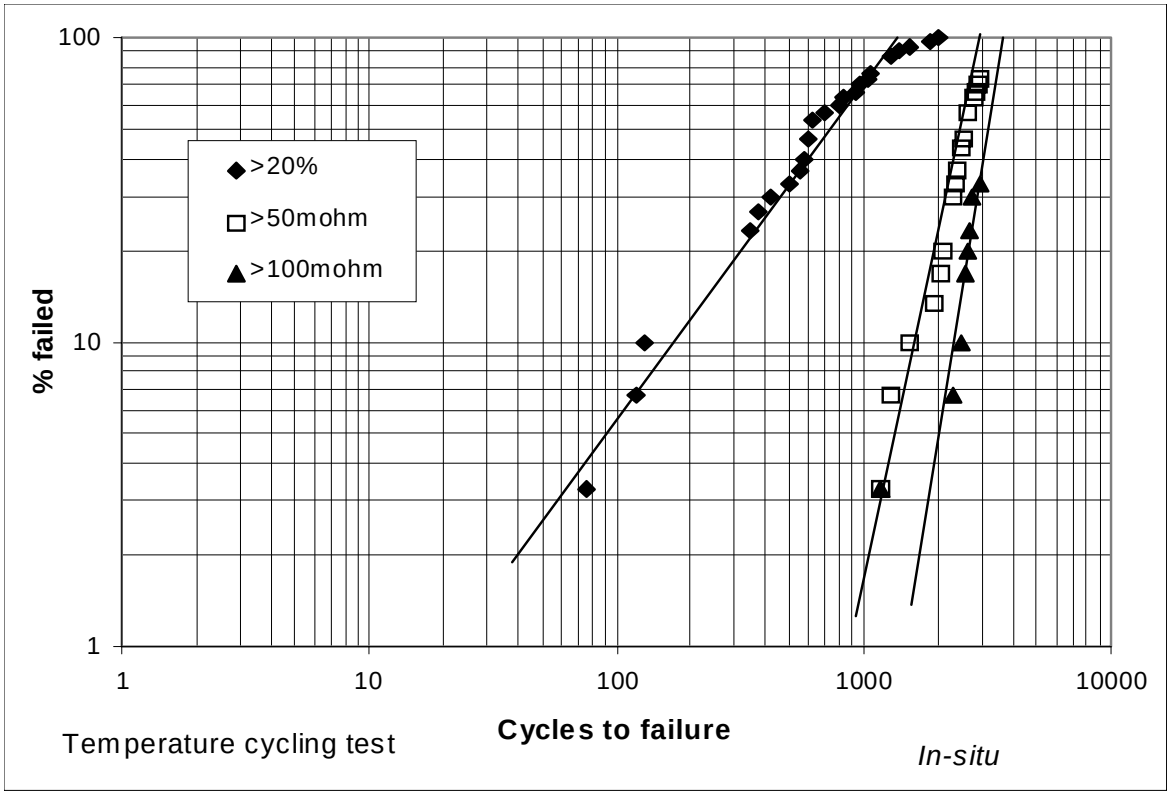

Figure 35. Cumulative failure of an epoxybased ACA joint in after a temperature cycling test from -40 to +125 degree C with a dwell time of 15 min at hold temperatures.

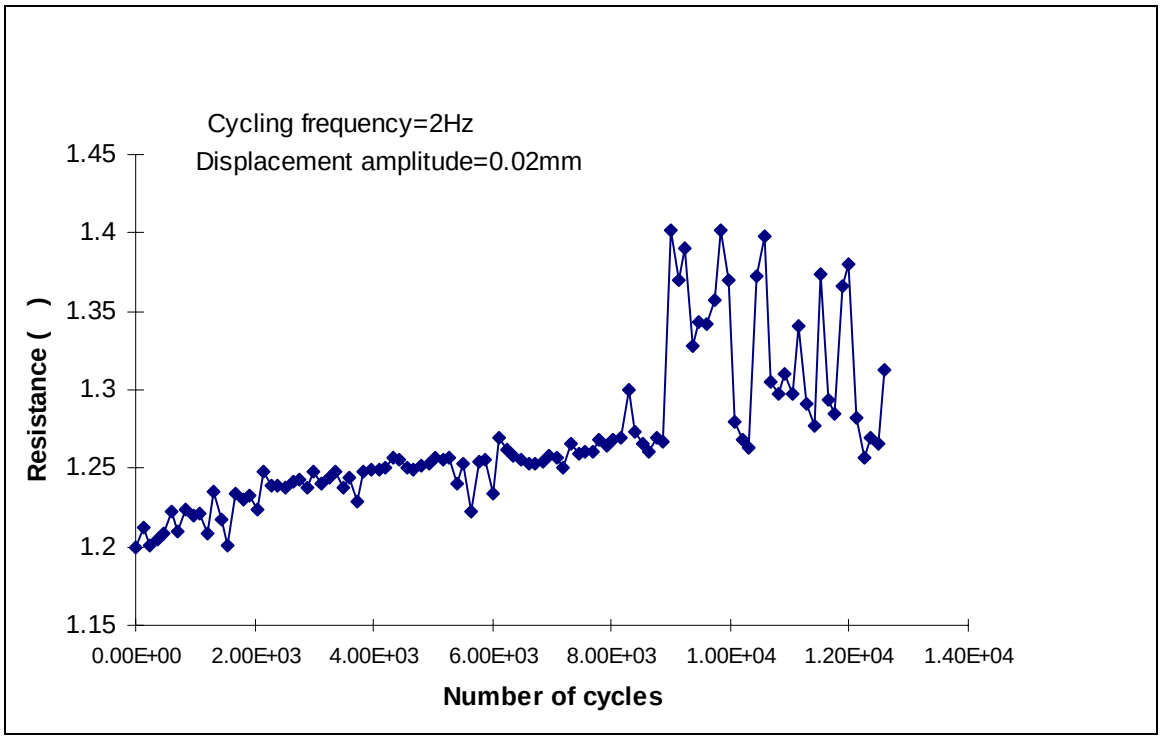

(a)

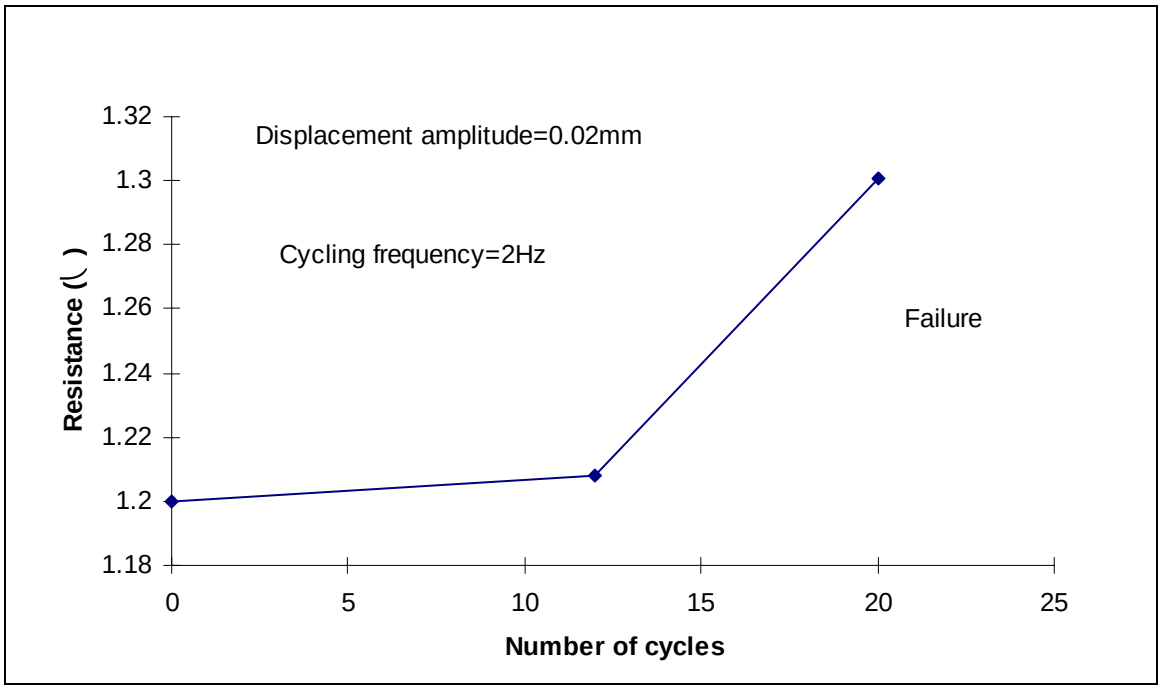

(b)

Figure 36. Electrical resistance of a daisy chain versus the number of cycles of low-cycle fatigue testing. (a) Dry environment; (b) 85°C and 85%RH [63].